THE JOURNAL OF PHYSICAL CHEMISTRY C

Article

pubs.acs.org/JPCC

Novel Reaction Mechanisms Pathways in the Electron Induced Decomposition of Solid Nitromethane (CH_3NO_2) and D3-Nitromethane (CD_3NO_2)

Ralf I. Kaiser* and Pavlo Maksyutenko

Department of Chemistry and W. M. Keck Research Laboratory in Astrochemistry, University of Hawaii at Manoa, Honolulu, Hawaii 96822, United States

ABSTRACT: Icy films of nitromethane (CH_3NO_2) together with D3-nitromethane (CD_3NO_2) were exposed to ionizing radiation to investigate the mechanisms in the decomposition of (D3)-nitromethane. The radiation induced modification of the ices was followed during the radiation exposure in situ via infrared spectroscopy (condensed phase) and via temperature-programmed desorption (TPD) exploiting reflectron time-of-flight mass spectrometry joined with single photon ionization of the subliming molecules at 10.49 eV (gas phase). The infrared spectroscopic and kinetics studies reveal the synthesis of methyl nitrite (CH_3ONO) via isomerization of nitromethane (CH_3NO_2) as well as the presence of the molecular (formaldehyde (H_2CO), nitrosylhydride (HNO)) and radical decomposition pathways (methoxy radical (CH_3O), nitrogen monoxide (NO)) accounting for about 85% of all products formed. Here, TPD studies exploiting reflectron time-of-flight mass spectroscopy together with single photon ionization exposed three classes of complex molecules: (i) nitroso compounds [nitrosomethane (CH_3NO), nitrosoethane (C_2H_5NO), nitrosopropane (C_3H_7NO)], (ii) nitrites [methylnitrite (CH_3ONO), ethylnitrite (C_2H_5ONO), propylnitrite (C_3H_7ONO], and (iii) higher molecular weight products with the synthesis of the homologues series of nitroso and nitrite compounds likely governed by a stepwise molecular growth via carbene (CH_2) insertion. Three decomposition pathways of nitromethane were identified, which do not take place in the gas phase: (i) the fragmentation of nitromethane to the nitromethyl radical (CH_2NO_2) plus suprathermal atomic hydrogen (H), (ii) formation of nitrosomethane (CH_3NO) plus atomic oxygen (O), and (iii) generation of singlet carbene (CH_2) plus nitrous acid (HONO) thus opening up mass growth processes, which are not feasible under collisionless conditions.

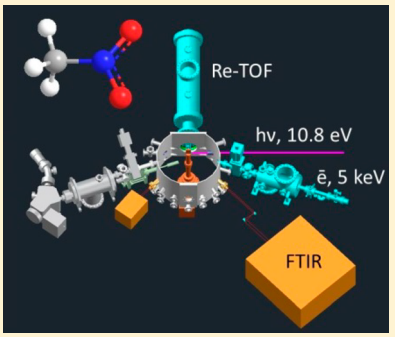

1. INTRODUCTION

Nitromethane (CH_3NO_2) is considered as a model of nitrohydrocarbon-based (RNO_2) energetic material covering propellants,[1,2] explosives,[3−6] and high-performance fuel additives for internal combustion engines and detonation systems.[7] Here, an intimate knowledge of the pathways in the (unimolecular) decomposition of nitromethane and of the succeeding reactions of the radicals formed in this process is crucial to foretell the aging behavior,[8,9] performance,[10,11] and the sensitivity to heat and shock of energetic materials.[9,12−20] These insights are further invaluable to dispose energetic materials safely under controlled conditions, to model the time-dependence during the ignition stage of explosives, and to develop novel insensitive energetic materials. The investigation of these decomposition processes still represents a substantial challenge for experimentalists, theoreticians, and modelers[21,22] considering the nonequilibrium conditions under which these reactions often occur.[23−34]

Therefore, the fragmentation pathways mechanisms of nitromethane (CH_3NO_2) have been comprehensively investigated in the gas phase utilizing and ultraviolet photodissociation (UVPD) and infrared multi photon dissociation (IRMPD) for the last three decades.[39−53] The experiments and computations exposed three channels: (1) the unimolecular decomposition of nitromethane (CH_3NO_2) to the methyl radical (CH_3) and to nitrogen dioxide (NO_2) (reaction 1) together with (2) a roaming-mediated nitromethane (CH_3NO_2)−methylnitrite (CH_3ONO) isomerization along with a unimolecular decomposition through (2a) a radical mechanism forming the methoxy radical (CH_3O) and nitrogen monoxide (NO) (reactions 2a and 2b) through a molecular elimination pathway resulting in formaldehyde (H_2CO) plus nitrosylhydride (HNO) (reaction 2b).[35−38,54−63] Nagata et al. proposed that multiphoton dissociation of nitromethane (CH_3NO_2) at 193 nm results in the formation of highly reactive carbene (CH_2) and methylidyne (CH) radicals from methyl radicals (CH_3) via two- and/or three-photon processes (reactions 3), respectively.[38]

$$CH_3NO_2 \rightarrow CH_3 + NO_2 \quad (1)$$

$$CH_3NO_2 \rightarrow CH_3ONO \rightarrow CH_3O + NO \quad (2a)$$

Special Issue: Steven J. Sibener Festschrift

Received: December 20, 2014
Revised: April 30, 2015
Published: May 4, 2015

DOI: 10.1021/jp5127267
J. Phys. Chem. C 2015, 119, 14653−14668

Scheme 1. Schematic Potential Energy Diagram of High and Low Energy Isomerization Pathways of Nitromethane (CH_3NO_2)[a]

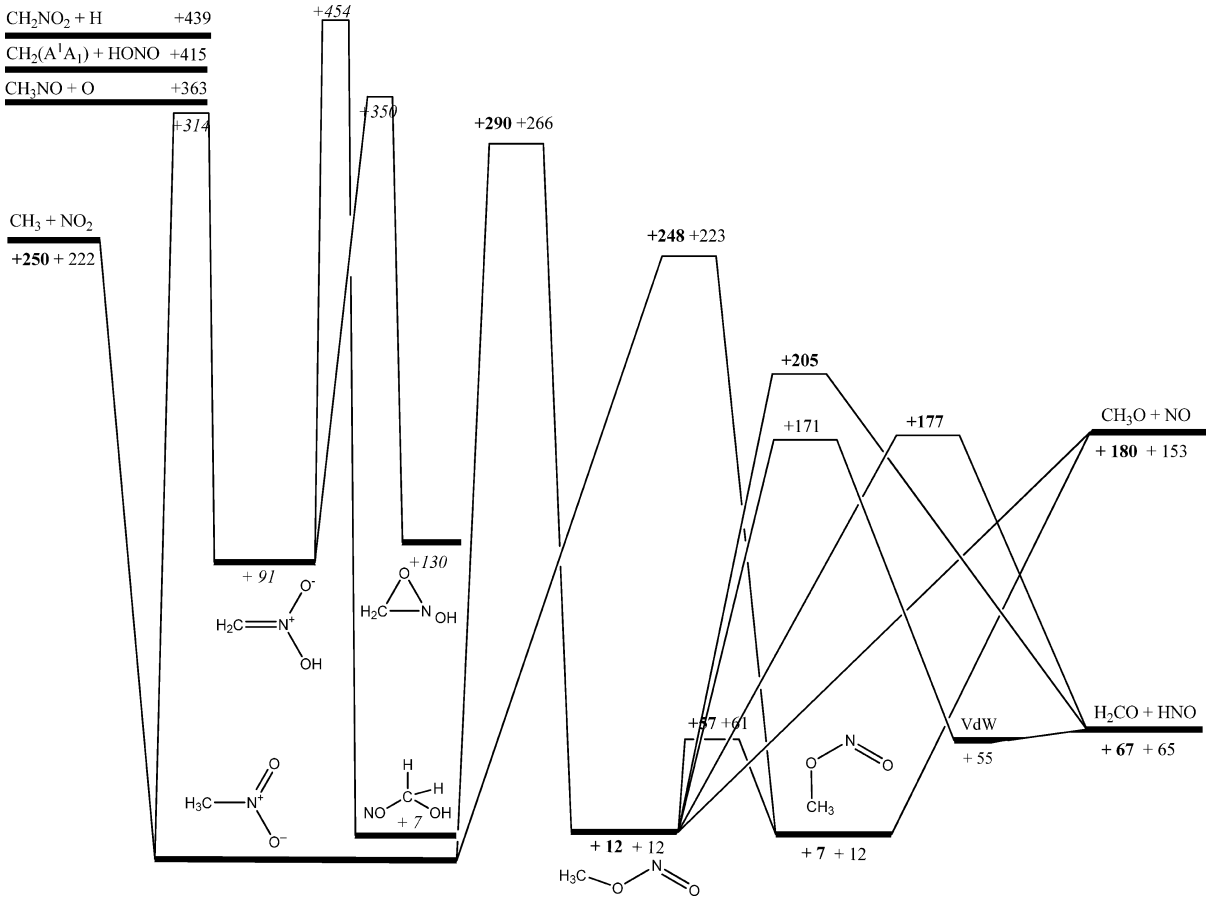

[a]Energies are given in kJ mol^{-1} and were compiled from Lin[117] et al. (bold) and McKee[64] (italics).

$$\rightarrow H_2CO + HNO \quad (2b)$$

$$CH_3NO_2 + h\nu \rightarrow CH_3 + NO_2 \quad (3a)$$

$$CH_3 + h\nu \rightarrow CH_2 + H \quad (3b)$$

$$CH_3 + h\nu \rightarrow CH + H_2/2H \quad (3c)$$

Note that alternative high energy pathways do not compete under IRMPD and UVPD conditions at wavelengths as low as 193 nm (Scheme 1). These involve a hydrogen atom migration via a barrier of 314 kJ mol^{-1} forming aci-nitromethane (H_2C═N(O)OH) (reaction 4) followed by an oxygen atom shift to form nitrosomethanol (H_2C(NO)OH) (reaction 5) or ring closure to *N*-hydroxyoxaziridene (c-CH_2NOH(O)) (reaction 6).[64] Finally, aci-nitromethane (H_2C═N(O)OH) might eliminate water (H_2O) to form isocyanic acid (HCNO) via a concerted molecular elimination pathway.

$$CH_3NO_2 \rightarrow H_2C{=}N(O)OH \quad (4)$$

$$H_2C{=}N(O)OH \rightarrow H_2C(NO)OH \quad (5)$$

$$H_2C{=}N(O)OH \rightarrow \text{c-}CH_2NOH(O) \quad (6)$$

In the solid state, only two experimental works exist. Broadband photolysis of nitromethane (240−360 nm) in an argon matrix at 14 and 20 K suggested the formation of *cis*- and *trans*-CH_3ONO as the primary pathway. On prolonged photolysis, these absorptions diminish in intensity, and there is continued growth in the absorptions of higher order products such as a formaldehyde (H_2CO)−nitrosylhydride (HNO)-bonded complex and also nitrosomethanol ($ONCH_2OH$).[65,66] A water (H_2O)−isocyanic acid (HCNO) complex was monitored at prolonged radiation exposure. Han et al.[67] and Chang et al.[68] probed the thermal decomposition of condensed phase nitromethane theoretically in molecular dynamics calculations.[67,68] These computations postulated a nitromethane (CH_3NO_2) to methyl nitrite (CH_3ONO) isomerization dominating at lower temperatures (2000−2500 K) and an intermolecular hydrogen atom transfer forming the CH_3NOOH isomer plus a nitromethyl (CH_2NO_2) radical at temperatures of about 3000 K (reaction 7). A hydrogen migration in nitromethane was also found to yield aci-nitromethane (H_2C═N(O)OH), which then ejects water (H_2O) to isocyanic acid (HCNO) (reaction 8).

$$CH_3NO_2 + CH_3NO_2 \rightarrow CH_3NOOH + CH_2NO_2 \quad (7)$$

$$CH_3NO_2 \rightarrow H_2C{=}N(O)OH \rightarrow HCNO + H_2O \quad (8)$$

Alternatively, the formation of water might involve intramolecular hydrogen atom transfers. In this process, the hydroxyl group (OH) is forecasted to commence from CH_3NOOH and the remaining hydrogen atom originates from formaldehyde (H_2CO). The authors concluded that besides these smaller molecules, the decomposition forms (hitherto unidentified) complex organic molecules containing up to 70% of the carbon and nitrogen of the nitromethane. Since the computations predict that on a time scale of 200 ps,

DOI: 10.1021/jp5127267
J. Phys. Chem. C 2015, 119, 14653−14668

only molecules holding a maximum of three carbon atoms are formed. Guo et al.[61] and Citroni et al.[69] predicted that the destruction of nitromethane likely implicates multi center pathways involving intramolecular hydrogen atom transfer and short-lived radicals along with complex molecules carrying the C−N−C−N-based chain moiety. Reed et al. conducted quantum molecular dynamics calculations mimicking condensed phase nitromethane (CH_3NO_2) during the explosion.[70,71] These calculations amplify the crucial mechanism of an intermolecular hydrogen atom shift from the methyl group to the oxygen atom to aci-nitromethane ($H_2C{=}N(O)OH$) (reaction 8). In conclusion, no coherent mechanisms have been untangled describing the decomposition of nitromethane along with the reactions of the carbon, nitrogen, and oxygen-bearing radical species generated in these processes.[68,69,72] Consequently, a novel experimental investigation of the decomposition of nitromethane in the condensed phase and the subsequent reaction pathways of the carbon, nitrogen, and oxygen-bearing radicals is required.

Here, we experimentally explore the underlying mechanisms of the decomposition of nitromethane (CH_3NO_2)—together with the fully deuterated counterpart (CD_3NO_2)—in a novel ultrahigh vacuum machine upon exposure to energetic electrons at 5 K and expose the primary reaction products. These experiments are carried out in the condensed phase at temperatures as low as 5 K exploiting energetic electrons depositing on average 4.1 ± 0.4 eV per CH_3NO_2 molecule. The decomposition of the precursor molecules (CH_3NO_2) and the successive radical reactions are traced spectroscopically via Fourier transform infrared (FTIR) spectroscopy in thin icy films on line and in situ during the electron exposure. These studies assist extracting concepts on the reaction mechanisms, products, and intermediates in the decomposition of nitromethane and of the radical reactions involved in the condensed phase. After the irradiation, the samples are warmed up and the subliming molecules are detected in the gas phase via two complementary methods: (i) quadrupole mass spectrometry via electron impact ionization (70 eV) of the neutral species and (ii) vacuum ultraviolet (VUV) single photon ionization of the subliming neutral molecules at 10.49 eV coupled with a reflectron time-of-flight mass spectrometer (ReTOFMS). These data ultimately aid the fundamental understanding of the nonequilibrium decomposition of energetic materials and inherent energy transfer processes involving the generation of carbon-, nitrogen-, and oxygen-centered radicals.

2. EXPERIMENTAL SECTION

2.1. Sample Preparation and Radiation Exposure. Briefly, the experiments were conducted in a ultrahigh vacuum (UHV) vessel (Figure 1)[75−77] evacuated to a base pressure of a few 10^{-11} Torr. A coldfinger is interfaced to a Sumitomo Heavy Industries helium refrigerator. A polished silver wafer is attached to the target and sandwiched with indium foil to maximize thermal conductivity. Cyrogenic solid films of nitromethane (CH_3NO_2, TCI AMERICA, ≥99%) and D3-nitromethane (CD_3NO_2, Sigma-Aldrich, ≥98% D) are deposited at 5.5 K via vapor deposition at a pressure (uncorrected for ion gauge sensitivity) of 5 × 10^{-8} Torr resulting in ices of 500 ± 10 nm thicknesses determined via laser interferometry exploiting a HeNe laser (632 nm).[78−82] Each ice was irradiated with 5 keV electrons at 5.5 ± 0.1 K for 1 h at electron currents of 15 nA by scanning the electron beam over an area of 1.0 ± 0.1 cm^2. The dose per molecule deposited

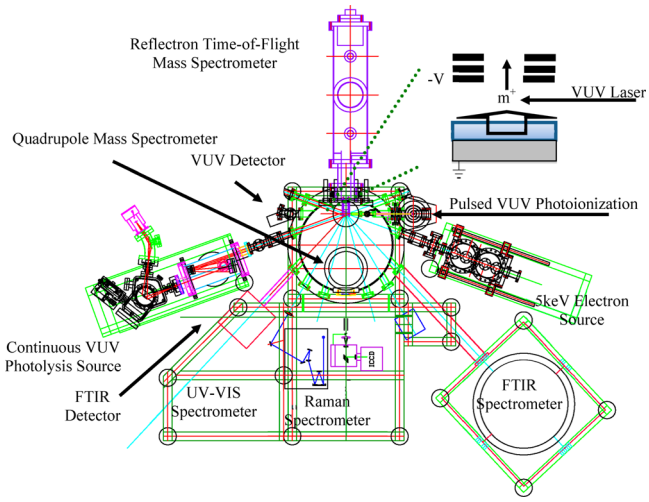

Figure 1. Schematic top view of the main chamber including the analytical instruments, radiation sources, and the cryogenic target (point of converging lines). The alignment of the cryogenic target, radiation sources, and infrared spectrometer allows simultaneous on line and in situ measurements of the modification of the targets upon the irradiation exposure. After the irradiation, the cold head can be rotated 180° to face the ReTOF mass spectrometer; the target can then be warmed up allowing the newly formed products to sublimate where upon they are photoionized and mass analyzed. The inset (top right) shows the geometry of the ReTOF ion source lenses with respect to the target and ionization laser.

was computed from Monte Carlo simulations (CASINO)[83] to be 4.1 ± 0.4 eV molecule at an irradiation currents of 15 nA, taking into consideration the scattering coefficient and the energy deposited from the backscattered electrons (Table 1).[75]

Table 1. Compilation of the Energy Fractions Extracted from the CASINO Calculations for a 15 nA Irradiation

back scatter energy (BSE) per electron	1.21 ± 0.12 keV
transmitted energy (TE) per electron	0.018 ± 0.001 keV
absorbed energy (AE) per electron	5 keV
fraction BSE ($f1$)	36 ± 5%
fraction TE ($f2$)	2 ± 1%
fraction AE ($f3$)	62 ± 5%
total dose keV/electron	4.6 ± 0.4
total electrons	3.4 × 10^{14}
average depth	371 ± 10 nm
density	1.117 g cm^{-3}
area processed	1.0 ± 0.1 cm^2
total number of molecules processed	4.1 × 10^{17}
dose per molecule	4.1 ± 0.4 eV per molecule

We utilize the latest version of CASINO (v2.42) to simulate the interaction of electrons and the energy loss processes with the nitromethane ices.[84] A simulation was performed for pure nitromethane (CH_3NO_2) with a thickness 500 nm as derived from the in situ laser interferometry. CASINO requires a priori knowledge of the densities and composition. This was estimated here via the Lorentz−Lorenz relation.[85] The Lorenz coefficient L is almost constant over a fixed wavelength. From the calculated refractive index and the densities, we obtain L = 0.217 cm^3g^{-1}. By substituting L and the refractive index n_f into the Lorentz−Lorenz relation (9)

$$L\rho = ({n_f}^2 - 1)/({n_f}^2 + 2) \quad (9)$$

DOI: 10.1021/jp5127267
J. Phys. Chem. C 2015, 119, 14653−14668

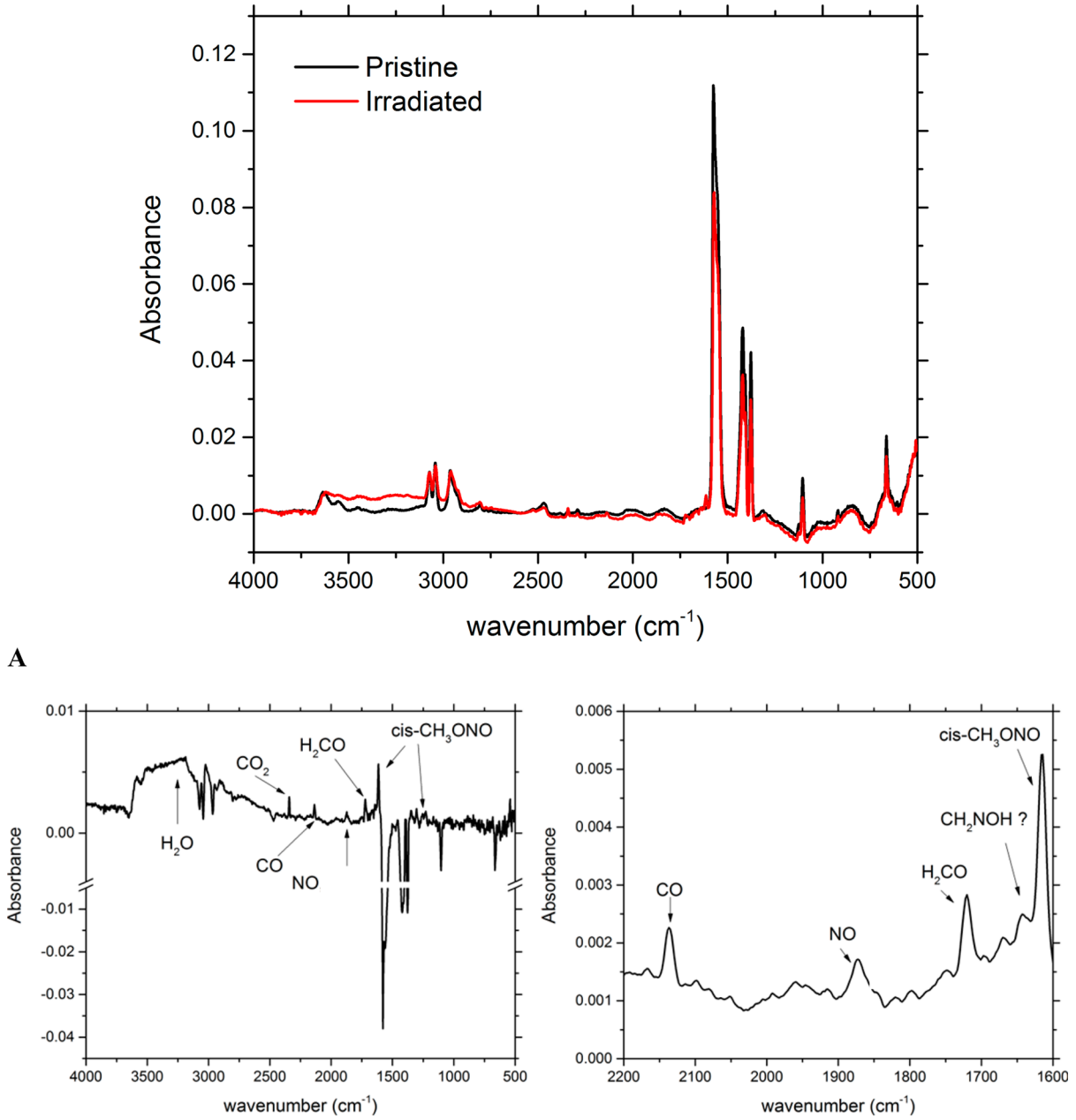

Figure 2. (A) Infrared spectra of the nitromethane ices at 5.5 K before (black) and after (red), irradiation at 15 nA. (B) Difference spectra of pristine and irradiated nitromethane ice at 5.5 K to highlight the subtle changes; shown on the right is an expanded view for clarity.

we calculate the density of nitromethane ice to be 1.117 g cm^{-3}. This density compares well to the density of pure nitromethane in the liquid phase with literature values of 1.137 g cm^{-3}.[82] Estimating the density of ices following this technique has been demonstrated previously by Modica et al. and Luna et al.[85,86] to be accurate within 20%. Within CASINO, electrons are simulated with kinetic energy of 5 keV to strike the surface of sample layer at an angle of 70° relative to surface normal; a total of 10^6 trajectories were used to simulate the energy transfer processes. These calculations result in an average dose of 4.1 ± 0.4 eV per molecule (see Table 1).

2.2. Analytical Techniques. For the on line and in situ identification of the newly formed species, FTIR spectroscopy was exploited in the range of 6000−500 cm^{-1} at a resolution of 4 cm^{-1} in intervals of 2 min resulting in 30 infrared spectra. After the irradiation, the sample was kept at 5.5 K for 1 h; then, temperature-programmed desorption (TPD) studies were carried out by heating the irradiated ices at a rate of 0.5 K min^{-1} to 300 K. The subliming molecules were photoionized via single photon ionization and probed in a reflectron time-of-flight mass spectrometer (ReTOF)[76] and a residual gas analyzer quadrupole mass spectrometer (QMS). For gas phase detection and mass analysis via ReTOF, the molecules were ionized following single photon ionization exploiting pulsed (30 Hz) coherent vacuum ultraviolet (VUV) light at 118.2 nm (10.49 eV).[75,87−89] Here, the third harmonic (354.6 nm) of a Nd:YAG laser (Spectra Physics, PRO − 250; 30 mJ per pulse) was exploited to produce the VUV photon utilizing xenon (Xe) gas as the nonlinear medium producing about 10^{13} photons cm^{-2} s^{-1} depicting a conversion efficiency of about 10^{-4} exploiting a

DOI: 10.1021/jp5127267
J. Phys. Chem. C 2015, 119, 14653−14668

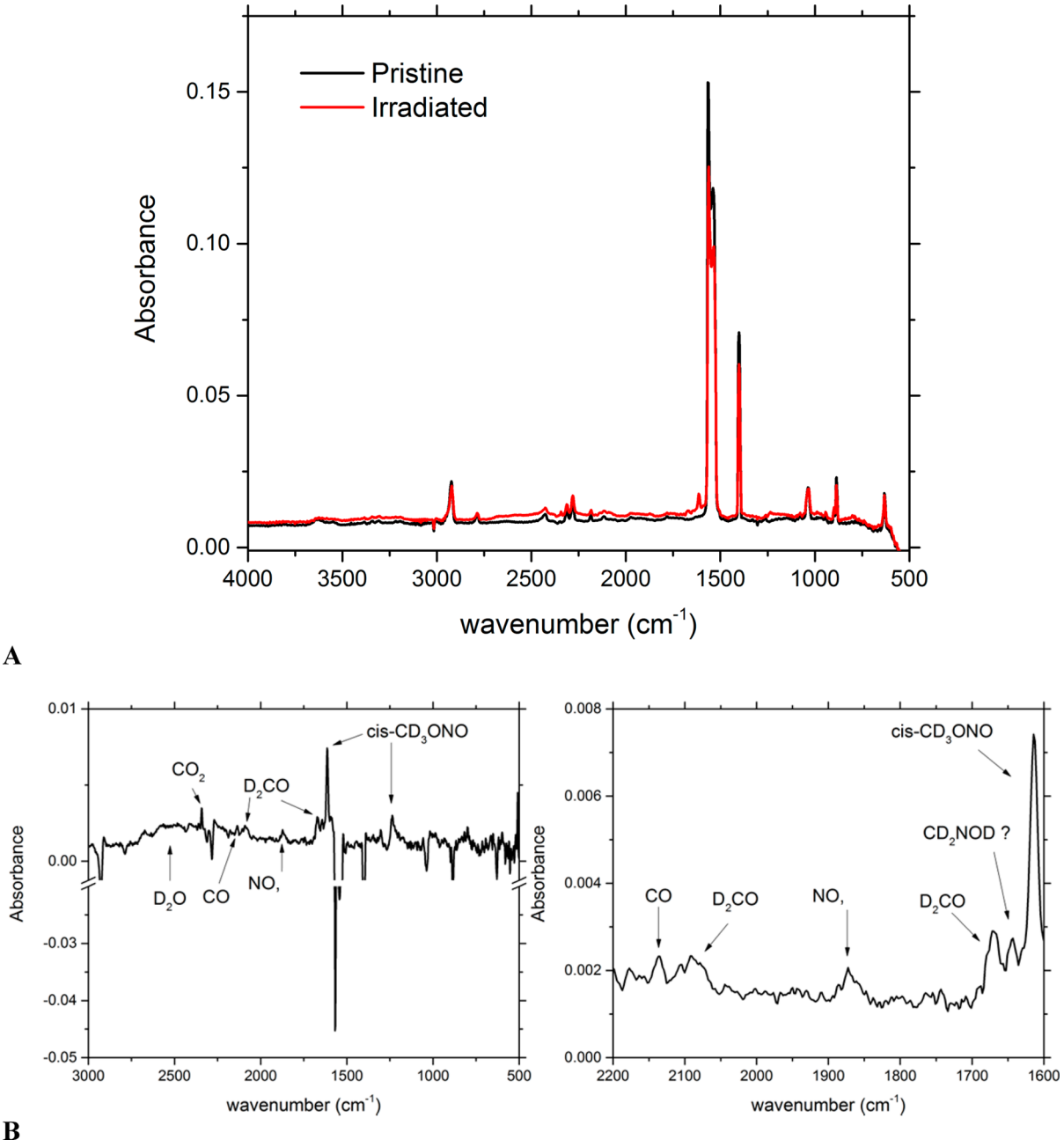

Figure 3. (A) Infrared spectra of the D3-nitromethane (CD_3NO_2) ices at 5.5 K before (black) and after (red) irradiation at 15 nA. (B) Difference spectra of pristine and irradiated D3-nitromethane ice at 5.5 K to highlight the subtle changes; shown on the right is an expanded view for clarity.

nonlinear four wave mixing process ($\omega_{vuv} = 3\omega_1$). The 10.49 eV light was separated exploiting an off-axis lithium fluoride (LiF) lens. The ions resulting from the photoionization were then extracted into a reflectron time-of-flight mass spectrometer whereupon the ions are mass resolved according to their arrival times.

3. RESULTS AND DISCUSSION

3.1. Infrared Spectroscopy. *3.1.1. Qualitative Analysis.* During the radiation exposure of the nitromethane and D3-nitromethane samples with energetic electrons, multiple new absorption features emerged (Figures 2 and 3). These could be assigned to small and discrete molecules (Table 2, Figures 2 and 3). The most intense band observed correlates with the formation of cis-methylnitrite (CH_3ONO/CD_3ONO), a structural isomer of the nitromethane reactant, detected via two absorptions at 1614/1614 cm^{-1} (ν_3) and 1227/1235 cm^{-1} (ν_6) based upon FTIR data of matrix isolated cis-CH_3ONO.[90] Less intense fundamentals overlap with the absorptions of the nitromethane matrix. Note, however, that nitrogen dioxide (NO_2) has a similar peak position at 1614 cm^{-1} with comparable band strength.[65,91] In addition, cyanic acid (NCOH) could account for the peak at near 1230 cm^{-1}.[92−94] Formaldehyde oxime (CH_2NOH/CD_2NOD)—a structural isomer of nitrosomethane (CH_3NO)—is tentatively assigned to the band observed at 1640 cm^{-1} based on literature value of 1640 cm^{-1} attributed to the CN stretching.[95] Other modes of formaldehyde oxime with similar intensity overlap with water and weak combination bands of nitromethane; as such, a definitive assignment is difficult to ascertain. Formaldehyde

DOI: 10.1021/jp5127267
J. Phys. Chem. C 2015, 119, 14653−14668

Table 2

(A) Fundamental Absorption Features Observed in the Nitromethane (CH_3NO_2) and D3-Nitromethane (CD_3NO_2) Ices before the Irradiation

CH_3NO_2			CD_3NO_2		
this work	literature value[65,82,90,91,118]	assignment	this work	literature	assignment
3074	3072	ν_1 (CH str (B_2) CH_3NO_2)	2281	2280	ν_2 (CD str (B_2) CD_3NO_2)
3041	3045	ν_1 (CH str (B_1) CH_3NO_2)	2184	2185	ν_{11} (CD str (A_1) CD_3NO_2)
2964	2958	ν_2 (CH str (A_1) CH_3NO_2)	1564	1567	ν_3 (NO str (B_2) CD_3NO_2)
1577	1571	ν_{11} (NO str (B_2) CH_3NO_2)	1403	1401	----
1425	1428	ν_4 (CH_3 bend (B_2) CH_3NO_2)	1076	1077	ν_1 (CD str (B_1) CD_3NO_2)
1380	1381	ν_5 (NO str (A_1) CH_3NO_2)	1035	1038	ν_5 (CD_3 bend (B_2) CD_3NO_2)
1124	1125	ν_6 (CH_3 rock (B_1) CH_3NO_2)	898	897	ν_6 (CD_3 rock (B_1) CD_3NO_2)
1105	1102	ν_{13} (CH_3 rock (B_2) CH_3NO_2)	632	-----	ν_8 (NO_2 bend (A_1) CD_3NO_2)
919	921	ν_7 (CN str (A_1) CH_3NO_2)	-----	-----	-----
663	660	ν_8 (NO_2 bend (A_1) CH_3NO_2)	-----	-----	-----

(B) New Absorption Features Observed in the Nitromethane (CH_3NO_2) Ice after the Irradiation with 15 nA of 5 keV Electrons

peak position (cm^{-1})	literature values	assignment	reference
3250	3280	ν_1 OH stretch (H_2O)	65,91
2340	2340	ν_3 CO stretch (CO_2)	65,91
2135	2140	ν_1 CO stretch (CO)	65,91
2260	2254	ν_2 asymmetric stretch (HNCO)	96
1870	1875	ν_1 NO stretch (NO)	65,91
1720	1720	ν_4 CO stretch (H_2CO)	65,91
1614	1614	ν_3 NO stretch (cis-CH_3ONO)	90
1227	1230	ν_6 CH_3 rock (cis-CH_3ONO)	90

(C) New absorption features observed in the D3-nitromethane (CD_3NO_2) ice after the irradiation with 15 nA of 5 keV electrons

peak position (cm^{-1})	literature values	assignment	reference
2560	2572	ν_1 OD stretch (D_2O)	91,119
2340	2340	ν_3 CO stretch (CO_2)	65,91
2135	2140	ν_1 CO stretch (CO)	65,91
2082	2072	ν_1 CD symmetric stretch (D_2CO)	65,91
1870	1875	ν_1 NO stretch (NO)	65,91
1670	1680	ν_4 CO stretch (D_2CO)	65,91
1614	1614	ν_3 NO stretch (cis-CD_3ONO)	65
1235	1230	ν_6 CD_3 rock (cis-CD_3ONO)	

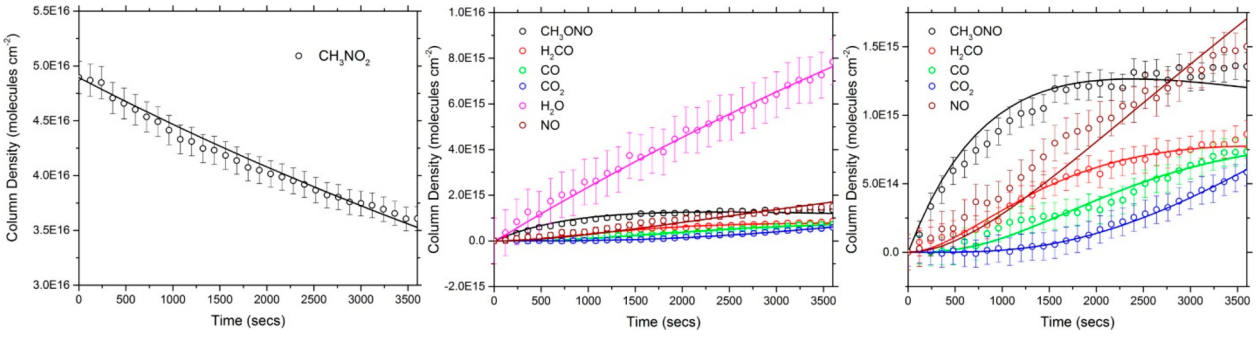

Figure 4. Temporal profiles of the determined column densities (circles) with fits of the of the reactant at 1380 cm^{-1} (CH_3NO_2) and of the products at 1614 cm^{-1} (CH_3ONO), 1720 cm^{-1} (H_2CO), 2135 cm^{-1} (CO), 2340 cm^{-1} (CO_2), 3280 cm^{-1} (H_2O), and 1872 cm^{-1} (NO) during the irradiation of solid nitromethane at 5.5 K.

(H_2CO/D_2CO) was detected at 1720/1670 cm^{-1} (ν_2) based on previously reported assignments.[65,82,91] In addition, simple carbon and nitrogen oxides were detected as well. Here, carbon monoxide (CO) and carbon dioxide (CO_2) were respectively monitored at 2140 cm^{-1} (ν_1) and 2340 cm^{-1} (ν_3) along with nitrogen monoxide (NO) at 1870 cm^{-1} (ν_1) in agreement with previous assignments of these molecules.[65,91] Isocyanic acid (HNCO) is assigned tentatively to a small peak at 2260 cm^{-1} (ν_2);[65,91] no other peaks were observed, as the most intense absorption was obscured by water and the amount formed was too low for detection above the noise limit with other vibrational bands.[96] Finally, water (H_2O/D_2O) was observed from the broad peak roughly centered at 3280/2560 cm^{-1} (ν_1), again, in agreement with previous assignments of energetically processed frozen nitromethane.[65,91]

3.1.2. Quantitative Analysis: Reaction Pathways. Having assigned the species synthesized from the radiolysis of nitromethane (Table 2), we are now elucidating the mechanisms associated with their formation. This is done by tracing the temporal profiles of the column densities of the

DOI: 10.1021/jp5127267
J. Phys. Chem. C 2015, 119, 14653−14668

newly formed molecules during the irradiation (Figure 4) and utilizing a set of coupled differential equations to numerically fit these profiles (Figure 5). The column densities were derived

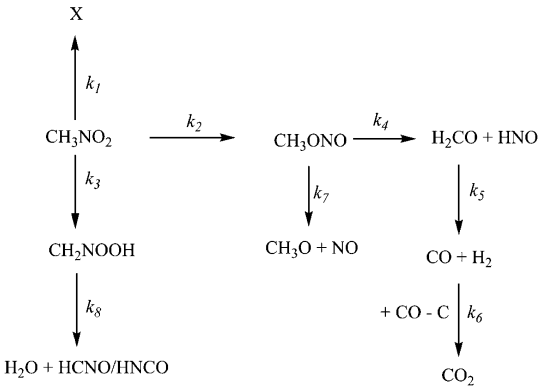

Figure 5. Overall kinetic scheme to fit the temporal evolution of the reactant and the newly formed products shown in Figures 3.

exploiting a modified Lambert–Beer law.[97−99] We would like to stress that the integrated absorption coefficients of the products formed during the irradiation are known from the literature. Here, the ν_3 (NO stretch) of methyl nitrite (CH_3ONO) holds a band strength of 2.8×10^{-17} cm molecule^{-1};[103] the ν_4 mode of formaldehyde has an integrated band strength of 9.6×10^{-18} cm molecule^{-1}, whereas carbon monoxide (CO) and carbon dioxide (CO_2) were quantified via their ν_1 and ν_3 fundamentals having integrated absorption coefficients of 1.1×10^{-17} cm molecule^{-1} and 1.6×10^{-17} cm molecule^{-1}, respectively. Water was probed using an integrated band strength of 2.0×10^{-16} cm molecule^{-1} in the area of 3600 to 2500 cm^{-1}.[104,105] Finally, the fundamental of nitrogen monoxide (NO) was quantified by exploiting an absorption coefficient of 6.8×10^{-18} cm molecule^{-1}.[106] A MATLAB script was written that was designed to solve the coupled differential equations as assuming all first-order kinetics utilizing optimized rate constants that minimized the error between the observed column densities and those predicted from the numerical solutions to the equations according to the reaction scheme shown in Figure 5. The resulting rate constants are listed in Table 3 for the nitromethane along with the numerical fits in

Table 3. Rate constants derived via solution of the reaction scheme depicted in Figure 5

reaction pathway	rate constant (s^{-1})
$CH_3NO_2 \rightarrow X$	$k_1 = 3.0 \pm 1.5 \times 10^{-6}$
$CH_3NO_2 \rightarrow CH_3ONO$	$k_2 = 3.7 \pm 0.4 \times 10^{-5}$
$CH_3NO_2 \rightarrow CH_2NOOH$	$k_3 = 5.1 \pm 0.6 \times 10^{-5}$
$CH_3ONO \rightarrow H_2CO + HNO$	$k_4 = 7.1 \pm 1.0 \times 10^{-4}$
$H_2CO \rightarrow CO + H_2/2H$	$k_5 = 1.1 \pm 0.4 \times 10^{-3}$
$CO + CO \rightarrow CO_2 + C$	$k_6 = 1.0 \pm 0.2 \times 10^{-3}$
$CH_3ONO \rightarrow CH_3O + NO$	$k_7 = 4.5 \pm 0.5 \times 10^{-4}$
$CH_2NOOH \rightarrow H_2O$ +HCNO/HNCO	$k_8 = 7.0 \pm 1.0 \times 10^{-2}$

plotted in Figure 4. We are aware that the interaction of ionizing radiation such as energetic electrons with low temperature solids can change the electronic structure of the ices. Further, a primary high energy electron can generate a cascade of secondary electrons within the sample as demonstrated by our CASINO calculations.[83] Therefore, the rate constants derived here have to be considered as "global" rate constants accounting for these accumulated effects. The infrared studies suggest that the response of the nitromethane by the energetic electrons is dictated by several key pathways: (i) the isomerization of nitromethane (CH_3NO_2) to methylnitrite (CH_3ONO) (k_2), (ii) the isomerization to aci-nitromethane ($H_2CN(O)OH$) (k_3) followed by a decomposition resulting in the formation of water (H_2O) and isocyanic acid (HNCO) and/or cyanic acid (HCNO) (k_8), and (iii) a less important, but required generic destruction pathway (k_1) of nitromethane to higher molecular weight products, which cannot be detected via infrared spectroscopy, to account for the mass balance as described below. Note that the sum of the rate constants of the isomerization of nitromethane to methylnitrite (CH_3ONO) and to aci-nitromethane ($H_2CN(O)OH$) is about 30 times higher compared to the conversion of nitromethane to higher molecular-weighted products. The production of methylnitrite is then followed by a branched reaction involving a decomposition via a molecular pathway (k_4) forming formaldehyde (H_2CO) plus nitrosyl hydride (HNO) and a radical fragmentation pathway (k_7) resulting in the production of methoxy (CH_3O) plus nitrogen monoxide (NO), respectively. Formaldehyde is then followed with a decomposition resulting in the formation of carbon monoxide (CO) plus atomic and/or molecular hydrogen.[97,98] Carbon dioxide is formed following a reaction of carbon monoxide with another excited state carbon monoxide as identified previously.[99] Considering the mechanisms, it is important to highlight that the decomposition and successive reactions can happen on the ground, but also on excited state surfaces. The present experiments alone cannot untangle the role of the ground versus excited state surface; therefore, term symbols have been omitted.

3.1.3. Quantitative Analysis: Mass Balance. Utilizing the experimentally derived integrated band strengths of nitromethane,[100] we determined the number of nitromethane molecules destroyed and converted into products as a result of exposure to the high energy electrons. From the modified Beers–Lambert law[101] with the integrated area of the ν_5 band (NO stretching) at 1380 cm^{-1} and the derived integrated band strength of 4.4×10^{-18} cm molecule^{-1}, the calculated initial column density is $4.9 \pm 0.2 \times 10^{16}$ molecules per cm^2 and $3.6 \pm 0.2 \times 10^{16}$ molecules per cm^2 post irradiation resulting in a total budget of $1.3 \pm 0.2 \times 10^{16}$ nitromethane (CH_3NO_2) molecules. Band areas can be changed by optical interference;[102] however, this issue is bypassed by integrating only weak bands, whose absorbance remains linear with the amount of ice deposited. Following this, we can calculate the number of molecules for each of the identified species formed for comparison. Considering the most prominent band identified post irradiation was attributed to the ν_3 (NO stretch) of methyl nitrite (CH_3ONO) and a calculated integrated band strength of 2.8×10^{-17} cm molecule^{-1},[103] the total number of molecules formed is $1.4 \pm 0.1 \times 10^{15}$ or approximately 2.9 ± 0.2% of nitromethane. The amount of formaldehyde produced was estimated using an integrated band strength of 9.6×10^{-18} cm molecule^{-1} for the ν_4 mode,[104] resulting in $8.6 \pm 1.0 \times 10^{14}$ molecules or 1.7 ± 0.2% of nitromethane. Column densities of carbon monoxide and carbon dioxide were extracted using integrated band strengths of 1.1×10^{-17} cm molecule^{-1} and 1.6×10^{-17} cm molecule^{-1} respectively[105] resulting in the total production of $7.5 \pm 1.0 \times 10^{14}$ carbon monoxide (CO) molecules and $6.7 \pm 1.0 \times 10^{14}$ carbon dioxide (CO_2)

DOI: 10.1021/jp5127267
J. Phys. Chem. C 2015, 119, 14653−14668

molecules. The amount of formed water was probed from integrating the broad feature from 3600 to 2500 cm^{-1} while correcting for the overlapping nitromethane bands in this region via integration of these peaks and subsequent subtraction. Exploiting a band strength of 2.0×10^{-16} cm $molecule^{-1}$ of water,[105] the total number of water molecules formed is calculated at $7.8 \pm 1.0 \times 10^{15}$. This is most likely an overestimate as isocyanic acid (HNCO) overlaps with this integrated band as well.[96] Finally, using an integrated band strength value of 6.8×10^{-18} cm $molecule^{-1}$ for the fundamental of nitrogen monoxide (NO),[106] and a band strength value of 1.6×10^{-16} for the ν_2 band of isocyanic acid (HCNO),[96] a final abundance of $1.5 \pm 0.5 \times 10^{15}$ nitrogen monoxide (NO) molecules and $9.8 \pm 1.0 \times 10^{12}$ isocyanic acid (HNCO) molecules has been determined, respectively. In summary, 85 ± 10% of the nitromethane molecules that were destroyed upon exposure to 5 keV electrons can be accounted for via small molecules with the dominant product channel being the formation of water.

3.2. Mass Spectroscopy. *3.2.1. Molecules Identified via FTIR.* From the determined number of nitromethane reactants converted into smaller molecules as stated above (85 ± 10%), it is evident that 15 ± 10% of nitromethane is also transformed into higher molecular weight diversity of products that was either formed in such a low abundance as to not be detected utilizing in situ FTIR spectroscopy or their vibrational modes have similar frequencies and are consequently masked. In an effort to identify these missing molecules, we turned our attention to their detection utilizing TPD techniques coupled with single photoionization reflectron time-of-flight mass spectroscopy (ReTOFMS) and a quadrupole mass spectrometer (QMS) operating in residual gas analyzer mode. Here, after the electron exposure of the icy films, the irradiated nitromethane and D3-nitromethane samples are warmed up with 0.5 K min^{-1} to 300 K. The photoionization laser (10.49 eV) intersects the subliming molecules perpendicularly 1 mm above the target in ReTOFMS. The resulting ion counts are compiled as a function of temperature and mass-to-charge ratios for all systems (Figures 6 and 7; Table 4). From the vast quantities of observed ion counts at distinct mass-to-charge ratios during TPD process from the irradiated sample as shown in Figures 2 and 3, it is apparent that the molecules identified via in situ FTIR spectroscopy alone cannot account for all of the observed molecules. This observation is further supported from the apparent "missing" molecules as concluded in the mass-balance quantification described above. Signal observed in the ReTOFMS yields information only relevant to the mass-to-charge ratio. In order to elucidate chemical structure, we can compare the sublimation profiles of the irradiated CH_3NO_2 ices to that of the CD_3NO_2 ices. As shown in Figure 6, there are in general four major sublimation events occurring at temperatures 100, 165, 230, and 280 K ± 2 K in both of the processed ice systems. For the sake of avoiding redundancy, we will be listing the peak sublimation temperatures without the associated error of ±2 K. As evident from Figures 6 and 7, the sublimation profiles for the majority of ionized species peak with the sublimation of the parent nitromethane matrix at 165 K (Figure 8). This behavior was observed previously and attributed to cosublimation of the matrix isolated products due to the inherent intermolecular—mainly dipole−dipole—interactions.[107,108] Similar instances are observed throughout the remaining heat ramp to 300 K and either stem from cosublimation of molecules with comparable heats of

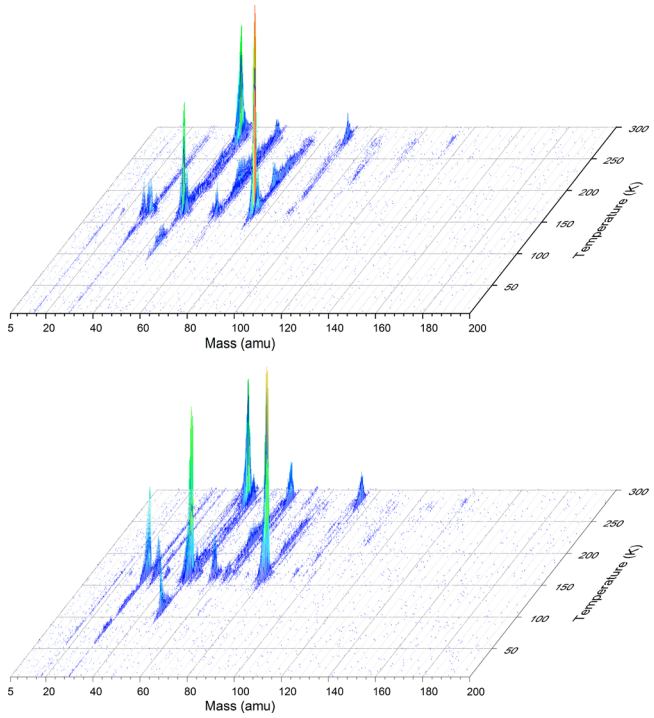

Figure 6. ReTOF photoionization spectra at a photon energy of 10.49 eV as a function of temperature of the newly formed products subliming into the gas phase from the irradiated nitromethane (CH_3NO_2; top) and D3-nitromethane (CD_3NO_2; bottom) ices.

desorption or in some cases fragmentation resulting from the ionization process. Let us focus our attention first on those reaction products observed via infrared spectroscopy (CH_3ONO, H_2CO, CO, CO_2, NO, H_2O, HNCO) (3.1.). Here, nitrogen monoxide (NO; ionization energy IE = 9.26 eV) could be identified via its signal at m/z = 30 in both the irradiated nitromethane and deuterated nitromethane ices. Note that the subliming nitromethane (CH_3NO_2) reactant cannot be photoionized since its ionization energy (11.08 eV)[109] is above the energy of the photoionization laser. In a similar fashion formaldehyde (H_2CO; IE = 10.88 eV),[109] carbon monoxide (CO; IE = 14.01 eV),[109] carbon dioxide (CO_2; IE = 13.77 eV), water (H_2O; IE = 12.62 eV), and isocyanic acid (HNCO; IE = 11.59 eV) are above the available ionization energy resulting in the lack of observed signal at the particular mass-to-charge ratios in the ReTOFMS analysis. However, methylnitrite (CH_3ONO), which presents the isomerization irradiation product of nitromethane, holds an ionization energy of only 10.44 eV[109] and can be photoionized. Therefore, the ion signal at m/z = 61 may originate from CH_3ONO^+; however, some sublimation events originate also from fragmentation of higher masses (see below). Furthermore, comparison of the TPD profile of ion signal at m/z = 61 (CH_3ONO) and 64 amu (CD_3ONO) should report similar sublimation rates if methylnitrite was indeed formed. As shown in Figure 7, the mass traces do not entirely overlap, implying that not only is methyl nitrite formed, but that fragmentation of higher molecular weight products also likely contributes.

3.2.2. Molecules without in Situ FTIR Identification. 3.2.2.1. Lower Molecular Weight Molecules. *cis*-Methylnitrite was found to fragment via a radical and molecular pathway (reaction 4) leading to a methoxy radical (CH_3O; 31 amu) plus nitrogen monoxide (NO; 30 amu) and formaldehyde (H_2CO;

DOI: 10.1021/jp5127267
J. Phys. Chem. C 2015, 119, 14653−14668

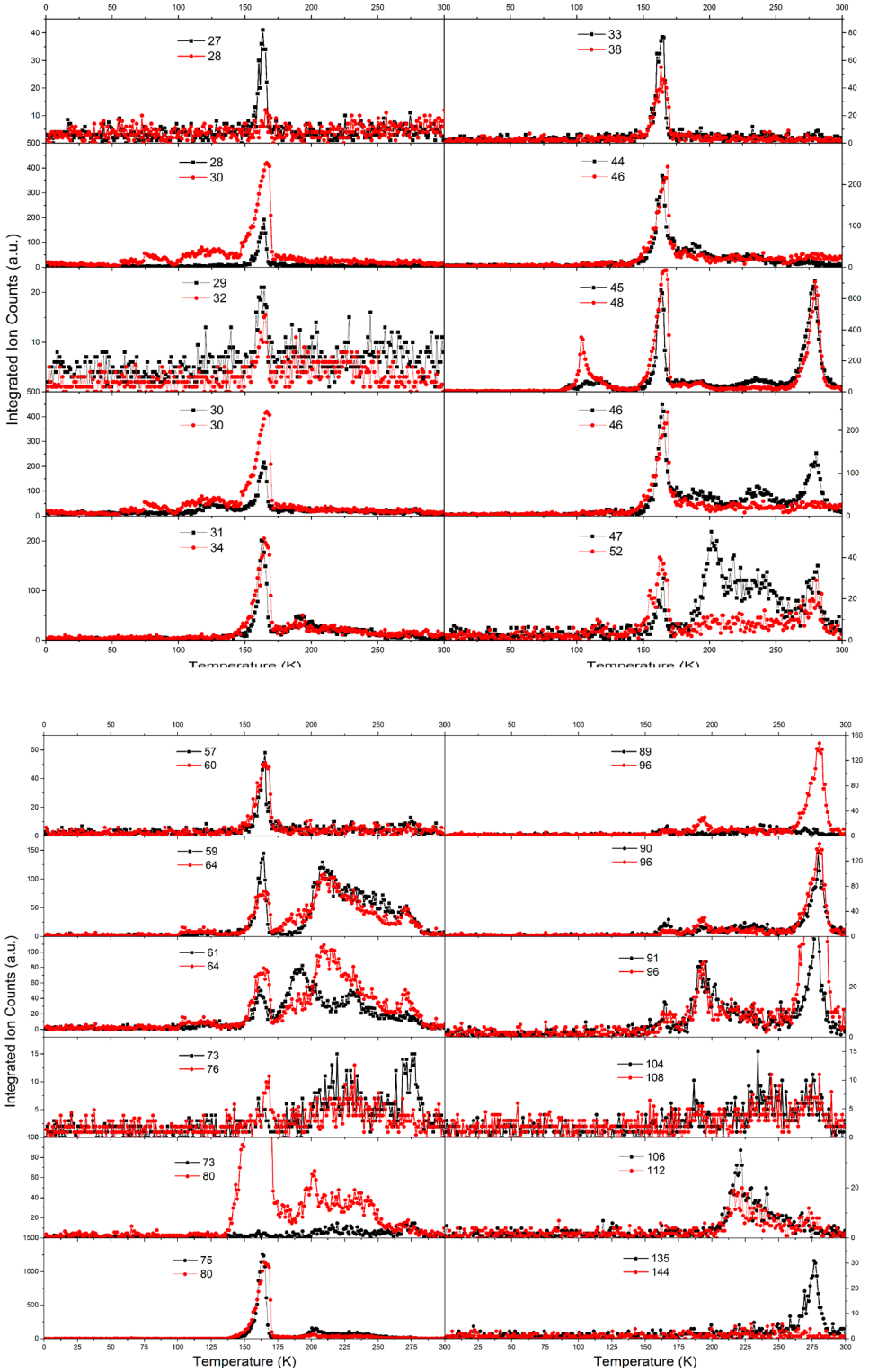

Figure 7. ReTOF sublimation profiles of the nitromethane ices processed via energetic electrons. Black squares correspond to those m/z ratios sublimating from CH_3NO_2 and red circles from CD_3NO_2.

30 amu) plus nitrosylhydride (HNO; 31 amu). As stated above, the radical pathway could be tracked down by nitrogen monoxide (IE = 9.26 eV) at about 165 K. The molecular channel as detected via formaldehyde (H_2CO; 30 amu) in the infrared can only be traced via the molecular ion of nitrosylhydride (HNO; 31 amu) and D1-nitrosylhydride (DNO; 32 amu) (IE = 10.1 eV). Recall that formaldehyde (IE = 10.9 eV) cannot be ionized in our setup (10.49 eV). Note that nitrogen monoxide (NO; 30 amu) also reacts with hydrogen atoms (H; 1 amu) to nitrosylhydride (HNO; 31 amu). Further, signal at m/z = 45 was assigned to nitrosomethane (CH_3NO; 45 amu; IE = 9.3 eV) likely formed via an atomic oxygen loss from nitromethane (CH_3NO_2; 61 amu); this process is endoergic by 363 kJ mol^{-1}. The formation of

DOI: 10.1021/jp5127267
J. Phys. Chem. C 2015, 119, 14653−14668

Table 4. Compilation of Product Classes Formed in the Photolysis of Nitromethane by Energetic Electrons[a]

Nitroso Compounds	Nitrite Compounds
CH_3NO (45 amu; *48 amu*)	CH_3ONO (61 amu; *64 amu*)
C_2H_5NO (59 amu; *64 amu*) C_2H_3NO (57 amu; *60 amu*)	C_2H_5ONO(75 amu; *80 amu*) C_2H_3ONO 73 amu; *76 amu*)
C_3H_7NO (73 amu; *80 amu*)	C_3H_7ONO (89 amu; *96 amu*)

Complex Products

$CH_3NONOCH_3$ (90 amu; *96 amu*)

$CH_3NONO_2CH_3$ (106 amu; *112 amu*)

$(CH_3NO)_3$ (135 amu; *144 amu*)

$CH_3OCH_2NO_2$ (91 amu; *96 amu*)

$ONCH_2CH_2NO_2$ (104 amu; *108 amu*)

Open Shell Reaction Intermediates

H, O, CH_2, CH_3O, NO, NO_2, CH_2NO, CH_2NO_2

[a]Compounds in italics are identified tentatively. Molecular weights of the products are given in parentheses; values in italics are for the fully deuterated products formed in the D3-nitromethane system.

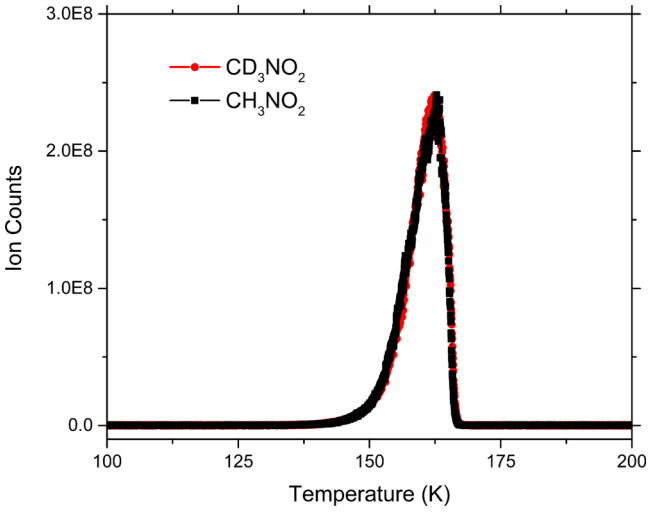

Figure 8. Sublimation profiles of nitromethane (CH_3NO_2) and D3-nitromethane (CD_3NO_2) as measured via the QMS showing the sublimation event of the parent at 165 K.

nitrosomethane can be matched based on the TPD profiled of the D3-nitromethane sample at m/z = 48 via the molecular ion peak of D3-nitrosomethane (CD_3NO; 48 amu); both TPD profiles at m/z = 45 and 48 for the processed nitromethane and D3-nitromethane sample agree nicely from 90−130 K, 140−175 K, 250−300 K.

The next group of mass peaks observed at this temperature correspond to m/z = 27, 28, and 29 amu in the processed CH_3NO_2 ice. Given the mass combinations and ionization energies we can effectively rule out carbon monoxide (CO; IE = 14.01 eV)[109] and molecular nitrogen (N_2; IE = 15.58 eV)[109] leaving the possibilities for molecular formulas to only include C, H, and/or N. As such, isomers of CHN, CH_2N, and CH_3N may explain the observed ion signal at m/z = 27, 28, 29 amu. The corresponding deuterated isomers would appear at m/z = 28, 30, and 32 amu, respectively. Given that closed shell isomers of CHN (hydrogen cyanide, hydrogen isocyanide) have ionization energies above 10.49 eV, no ion signal should appear. As such, these peaks are suggested to be the result of photofragmentation of the cosublimating higher mass organics (see below). Unfortunately, a direct comparison at m/z = 28 amu (CH_2N) and m/z = 30 amu (CD_2N) cannot be made as the dominant ion signal at m/z = 30 is attributed to nitric oxide as described above. Other possibilities for the these masses maybe attributed to the vinyl radical (C_2H_3, IE ≤ 8.59 eV),[109] ethylene (C_2H_4; IE = 10.51 eV),[109] or the ethyl radical (C_2H_5; IE = 8.12 eV).[109] These molecular formulas were discounted, however, as the TPD profiles did not match the deuterated counter parts. In regards to CH_3N isomers, methenamine (CH_2NH, IE = 9.88 eV)[109] is the only stable closed shell species in contrast to the associated radical. As we cannot completely negate VUV photoinduced fragmentation of the gas phase molecules, we are proposing these mass peaks to have molecular formula of CH_xN resulting from fragmentation of higher mass organics and/or possibly fragmentation of methenamine resulting in methylene amidogen radical (CH_2N, IE = 9.4 eV)[109] and CHN radical as these mass fragments were not seen in the TPD spectra of the pristine ices.

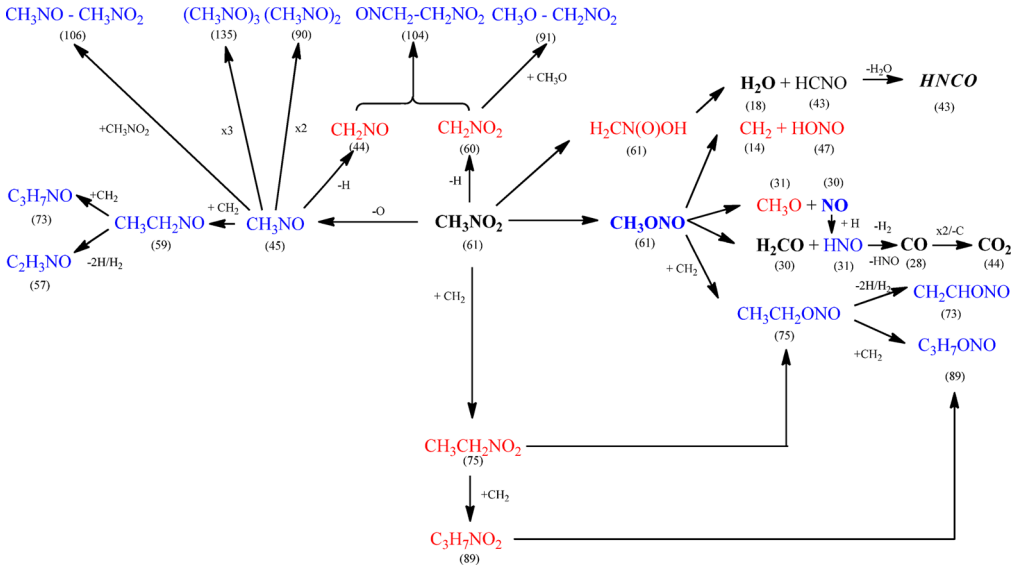

Figure 9. Reaction mechanisms taking place in nitromethane (CH_3NO_2) ice film under exposure to energetic electrons. Bold: infrared detection; blue: ReTOF detection; red: inferred reaction intermediates.

DOI: 10.1021/jp5127267
J. Phys. Chem. C 2015, 119, 14653−14668

Finally, the ion signal at m/z = 46 amu has been attributed to nitrogen dioxide (NO_2) as the TPD profile in the deuterated nitromethane ice is equivalent during the sublimation of the parent at 165 K. However, the ion signals at m/z = 46 and 50 amu match perfectly at all sublimation events after the parent (Figure 10), implying that the chemical formula has four

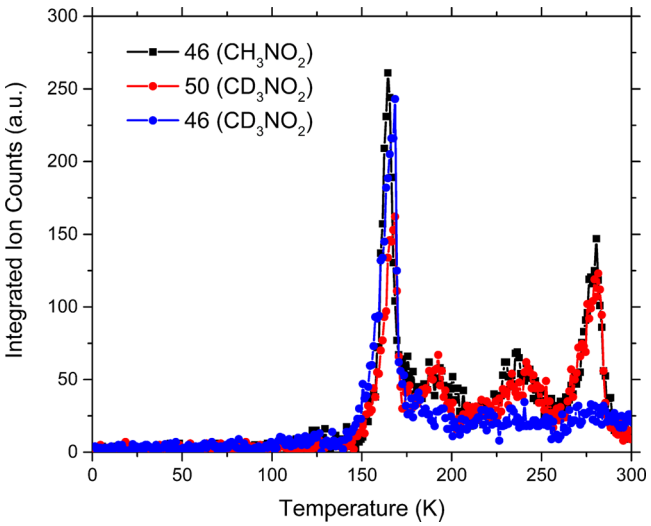

Figure 10. ReTOF TPD profiles monitored at m/z = 46 and 50. Nitrogen dioxide has been assigned to the peak at 165 K cosublimating with nitromethane (black square) as this ion signal was similar to that observed in CD_3NO_2 (blue circles). However, nitrogen dioxide cannot explain the remaining sublimation events. As such, we are attributing these peaks to be a consequence of photofragmentation of higher molecular weight products (see text).

hydrogen associated with this mass. As such, the observed sublimating masses may correspond to CH_3NOH^+, which is a result of fragmentation from higher mass organics (see below). Similar observations hold true for the remaining masses (33 vs 38; 44 vs 46; 47 vs 52). Based on previous UV photodissociation studies, we can suggest that the NO_2 fragment is produced in the gas phase in an excited state that decomposes to NO and O,[31,53,60] which is then subsequently ionized. Note that ion signal at m/z = 16 amu is not observed, as the ionization energy of oxygen atom is significantly above the threshold of this experimental setup at 13.6 eV.[109]

3.2.2.2. Complex Organic Molecules Originating from Carbene Reactions. The TPD data and the mass-to-charge ratios of the ionized products disclose a molecular mass growth process by 14 amu (nitromethane ice) and 16 amu (D3-nitromethane ice). This might be a consequence of a mass growth through reactions of precursor molecules with carbene (CH_2) and D2-carbene (CD_2), respectively. This process is apparent from signal probed at m/z = 45 versus 59 and 61 versus 75 from the nitromethane samples, which is also correlated with m/z = 48 versus 64 and 64 versus 80 in the D3-nitromethane ices. Here, singlet carbene *inserts* without barrier into the carbon–hydrogen bond of the methyl group of nitrosomethane (CH_3NO; 45 amu) yielding nitrosoethane (CH_3CH_2NO; 59 amu; IE = 10.1 eV). In the D3-nitromethane system, this shifts from D3-nitrosomethane (CD_3NO; 48 amu) to D5-nitrosoethane (CD_3CD_2NO; 64 amu) and results in a mass difference of 5 amu as a consequence of five deuterium atoms instead of hydrogen. Also, singlet carbene inserts into the carbon–hydrogen bond of methylnitrite (CH_3ONO; 61 amu) forming ethylnitrite (CH_3CH_2ONO; 75 amu) as verified in the D3-nitromethane system via the observation of D3-methyl nitrite (CD_3ONO; 64 amu) and D5-ethylnitrite (CD_3CD_2ONO; 80 amu) formed via D2-carbene insertion. Ethylnitrite holds an ionization energy of 10.53 eV slightly above the photon energy of 10.49 eV; nevertheless,[76] the electric fields of the extraction plate can lower the ionization energy (Stark effect)[110] by at least 0.04 eV. Ethylnitrite (CH_3CH_2ONO; 75 amu) may also be synthesized via carbene reaction with nitromethane giving nitroethane ($CH_3CH_2NO_2$), which then isomerizes to ethylnitrite (CH_3CH_2ONO; 75 amu). The TPD profiles of 59 and 64 ((D5)nitrosoethane) and 75 and 80 ((D5)ethylnitrite) agree well.

The weak signal at m/z = 89 might be rationalized by a successive mass growth process involving another carbene with nitroethane ($CH_3CH_2NO_2$; 75 amu) or ethylnitrite (CH_3CH_2ONO; 75 amu), yielding nitro(iso)propane ($C_3H_7NO_2$; 89 amu) or (iso)propylnitrite (C_3H_7ONO; 89 amu). Based on the ionization energies, propylnitrite (IE = 10.34 eV) and isopropylnitrite (IE = 10.23 eV) can be photoionized, but neither nitropropane (IE = 10.78 eV) nor isonitropropane (IE = 10.74 eV) can. It is important to point out that the signal in the D3-nitromethane at m/z = 96 is too high to connect with the synthesis of only D7-(iso)-propylnitrite. Therefore, a hitherto unassigned molecule must account for this signal, too. The signal at m/z = 73 could originate from a successive mass growth via carbene reaction with nitrosoethane (CH_3CH_2NO; 59 amu) synthesizing nitroso(iso)propane (C_3H_7NO; 73 amu). The corresponding signal in the D3-nitromethane system at m/z = 80 is dominated by D5-ethylnitrite (CD_3CD_2ONO; 80 amu), and a definite assignment is not feasible at the present stage. It is important to note that the signal at m/z = 73 could also be explained via molecular hydrogen elimination from ethylnitrite (CH_3CH_2ONO; 75 amu) forming vinylnitrite (C_2H_3ONO; 73 amu). The ionization energy of the nitroethylene isomer ($C_2H_3NO_2$; 73 amu) of 11.0 eV is too high to be ionized under the present experimental conditions. A hydrogen elimination in nitrosomethane (CH_3CH_2NO; 59 amu) may result in the signal at m/z = 57 (nitrosoethylene; 57 amu) correlated with the signal at m/z = 60 (D3-nitrosoethylene; 60 amu) in the exposed D3-nitromethane sample.

How can singlet carbene be formed? Previous experiments in our laboratory probing the interaction of ionizing radiation with solid methanol (CH_3OH),[97,98] methylamine (CH_3NH_2),[111] and ethane (CH_3CH_3)[112] revealed the presence of methane (CH_4) via retro-insertion of singlet oxygen atoms (O), singlet nitrene (NH), and singlet carbene (CH_2). If this pathway is also valid for nitromethane, retroinsertion of singlet carbene form nitrous acid (HONO; 47 amu). The ionization energy of the latter of 11.3 eV is higher than the 10.49 eV utilized in our studies. The formation of carbene and nitrous acid requires 415 kJ mol^{-1}; this energy can be covered by the energetic electrons easily.

3.2.2.3. Higher Molecular Weight Molecules Derived from Two Nitromethane Molecules. Higher molecular weight products from 90 to 106 amu can be rationalized by the involvements of formally two nitromethane molecules. First, upon exposure to energetic electrons, nitromethane (CH_3NO_2; 61 amu) and nitrosomethane (CH_3NO; 45 amu) can emit a hydrogen atom yielding the nitromethyl (CH_2NO_2; 60 amu) and nitrosomethyl (CH_2NO; 44 amu) radicals. These decompositions products are endoergic by 439 kJ mol^{-1} and

DOI: 10.1021/jp5127267
J. Phys. Chem. C 2015, 119, 14653–14668

245 kJ mol^{-1}, which can be overcome by the energetic electrons. These radicals react forming a species of the chemical formula $C_2H_4N_2O_3$. Based on a radical−radical recombination, this molecules could be 1-nitroso-2-nitroethane ($ONCH_2CH_2NO_2$; 104 amu). Due to the lacking signal in the D3-nitromethane system at m/z = 108, this assignment is tentative. Also, we probed the minor signal at m/z = 91 resulting from the reaction of nitromethyl (CH_2NO_2; 60 amu) with the methoxy radical (CH_3O; 31 amu) to methoxynitromethanol (CH_3O CH_2NO_2; 91 amu). The sublimation from 175 to 220 K in the D3-nitromethane ice at m/z = 96 amu ($CD_3OCD_2NO_2$) verifies this conclusion. Also, we probed the signals at m/z = 90 and 106. This can be attributed to dimers of nitrosomethane (i.e., CH_3NO−CH_3NO; 90 amu; IE = 8.6 eV), and of reaction products of nitrosomethane (CH_3NO; 45 amu) with nitromethane (CH_3NO_2; 61 amu) forming CH_3NO−CH_3NO_2 (106 amu). Nitrosomethane (CH_3NO) dimerizes easily forming (E)-azodioxymethane;[113] this reaction could also take place in the condensed phase via exposure to energetic electrons. The TPD profile at m/z = 90 hints to two sublimation events: 175 to 250 and 250 K to 300 K. The sublimation from 250 to 300 K correlated with m/z = 45, i.e., the nitrosomethane monomer, thus indicating that, upon photoionization, the cation dissociates to singly ionized nitrosomethane monomer as well. Data in the D3-nitromethane ice at m/z = 96 shifts the mass-to-charge by 6 amu; this confirms the presence of six hydrogen/deuterium atoms in the molecules at 90 amu (nitromethane system) and 96 amu (D3-nitromethane system). The signal at m/z = 106 is formally derived from reaction of a nitrosomethane (CH_3NO; 45 amu) with nitromethane (CH_3NO_2; 61 amu) yielding CH_3NO−CH_3NO_2 (106 amu). The TPD profiles of the nitromethane and D-nitromethane systems at m/z = 106 and m/z = 112 agree well, proposing that this molecule contains six hydrogen/deuterium atoms.

3.2.2.4. Higher Molecular Weight Molecules Derived from Three Nitromethane Molecules. In the electron-irradiated nitromethane system, the signal at m/z = 135 represents the highest ion observable. This can be assigned to a "trimer" of nitrosomethane (CH_3NO; 45 amu) of hitherto unknown structure. However, the signal is very weak, and no corresponding mass shift in the D3-nitromethane system by 9 amu, i.e. $(CH_3NO)_3$ versus $(CD_3NO)_3$, could be monitored. Therefore, this assignment must be considered as tentative.

4. SUMMARY AND CONCLUSIONS

The present study examined the energetic processing of solid nitromethane upon bombardment with energetic electrons at cryogenic temperatures and probed the newly formed molecules via two complementary techniques: FTIR and ReTOFMS. First we investigated the newly emerging infrared absorption bands qualitatively and assigned their carriers. Having detected multiple newly formed molecules in the irradiated nitromethane ices (CH_3ONO, H_2CO, CO, CO_2, NO, H_2O; tentatively HNCO and CH_2NOOH) on line and in situ, we also elucidated the underlying formation pathways. First, the temporal profiles and the kinetic fits suggest (pseudo) first-order kinetics of the formation of methyl nitrite (CH_3ONO) via isomerization of nitromethane (CH_3NO_2). Second, our studies proposed two competing pathways of the decomposition of methyl nitrite (CH_3ONO) into formaldehyde (H_2CO) plus nitrosyl hydride (HNO) and the methoxy radical (CH_3O) plus nitrogen monoxide (NO). This mechanism is consistent with the gas phase works[50] and also in computations.[59] Further theoretical calculations were also performed recently by Homayoon and Bowman,[114] confirming the existence of these fragmentation channels. Third, our data analysis suggests first-order kinetics of the formation of methyl nitrite (CH_3ONO) via isomerization of nitromethane (CH_3NO_2) in the condensed phase. This pathway was predicted by theory[115] and confirmed experimentally that isomerization to methyl nitrite (CH_3ONO) is in competition with the fragmentation of nitromethane.[50,116] The energized nitromethane initially enters the dissociation channel $CH_3\cdots NO_2$ with the calculated C−N bond length at about 4.58 Å.[114] The incipient fragments reorient and recombine to transiently form the *cis*-CH_3ONO isomer via roaming,[35−38,73,74] which can then result in the molecular and radical fragmentation pathways as discussed above (reaction 4). However, in the ice, the methyl radical and the nitrogen dioxide are trapped within the matrix cage and recombine back either to nitromethane (CH_3NO_2) or methyl nitrite (CH_3ONO). *In the condensed phase, roaming reaction dynamics are not required to explain the experimental data*. This "cage effect" is reflected in reaction mechanisms that do not exist in gas phase reactions under single collision conditions, where the nascent products "fly apart" or undergo prior reactions via "roaming". However, in the solid state, the internal energy of this intermediate is transferred to the surrounding matrix via phonon interaction; the solid acts like a "catalyst" in forming a product that cannot be synthesized in the gas phase. This is important in stabilizing the newly formed molecules in the solid phase and can lead to reaction products distinct from those in gas phase reactions under single collision conditions. Finally, to adequately fit the column densities of methyl nitrite, it was important to add an unknown decomposition pathway of nitromethane. Justification of this premise can be found in both the mass balance quantification and the proposed reaction pathways identified from the mass spectroscopic data that about 15 ± 10% of the nitromethane molecules had to be converted to higher molecular weight products.

These complex products were detected via ReTOFMS-PI. Three major product classes were assigned (Figure 9, Table 4) formally needing up to three nitromethane "building blocks": (i) nitroso compounds, (ii) nitrite compounds, and (iii) higher molecular weight molecules. First, a key molecular mass growth processes was attributed to insertion of carbene (CH_2) into carbon−hydrogen bonds forming from nitrosomethane (CH_3NO) a homologues series of *nitrosoalkanes*: nitrosoethane (C_2H_5NO) and nitrosopropane (C_3H_7NO). Also, starting with methylnitrite (CH_3ONO), carbene insertions leads to a homologues series of *nitritoalkanes*: ethylnitrite (C_2H_5ONO) and propylnitrite (C_3H_7ONO). Both C_2H_3NO and C_2H_3ONO are likely synthesized by hydrogen loss from their nitrosomethane (C_2H_5NO) and ethylnitrite (C_2H_5ONO) precursors. Second, we identified molecules that necessitate the reaction of (fragments of) two nitromethane building blocks: $CH_3NONOCH_3$, $CH_3NONO_2CH_3$, and tentatively $CH_3OCH_2NO_2$ as well as $ONCH_2CH_2NO_2$. The formation of $CH_3NONOCH_3$ and $CH_3NONO_2CH_3$ requires two neighboring nitrosomethane and nitrosomethane/nitromethane molecules—pathways that have been postulated previously.[68,72] Third, a hitherto unidentified "trimer" of nitrosomethane (CH_3NO)3 could be identified tentatively. Finally, the reactions in the condensed phase require initial decomposition pathways, which have not been monitored in

DOI: 10.1021/jp5127267
J. Phys. Chem. C 2015, 119, 14653−14668

previous gas phase experiments. These are the decomposition of nitromethane to the nitromethyl radical (CH_2NO_2) plus atomic hydrogen (H), (reaction 10), to nitrosomethane (CH_3NO) plus atomic oxygen (O) (reaction 11), and to singlet carbene (CH_2) plus nitrous acid (HONO) (reaction 12). These pathways are highly endoergic, but could be opened up by the interaction of energetic electrons with nitromethane molecules in the condensed phase.

$$CH_3NO_2 + h\nu \rightarrow CH_2NO_2 + H \quad \Delta_R G = +439\ \text{kJ mol}^{-1} \tag{10}$$

$$CH_3NO_2 + h\nu \rightarrow CH_3NO + O \quad \Delta_R G = +363\ \text{kJ mol}^{-1} \tag{11}$$

$$CH_3NO_2 + h\nu \rightarrow CH_2 + HONO \quad \Delta_R G = +415\ \text{kJ mol}^{-1} \tag{12}$$

In summary, our investigations unraveled that about one-fourth of the nitromethane molecules are converted to three product classes, which are not observable in classical gas phase experiments. These are (i) nitroso compounds, (ii) nitrite compounds, and (iii) complex higher molecular weight molecules. Finally, the present research represents a vastly undersized understanding to a very multifaceted issue that has only been skimmed over in the gas phase. Further analysis on the decomposition of nitromethane is absolutely critical in order to understand the full complexity of the process. These experiments will rely on the coherent use of molecular selective ionization utilizing tunable vacuum ultraviolet light and *ab initio* calculations as the decomposition of nitromethane in the solid state obviously results in molecules whose ionization energies have yet to be examined experimentally.

AUTHOR INFORMATION

Corresponding Author

*Tel: (808) 956-5731, E-mail: ralfk@hawaii.edu.

Notes

The authors declare no competing financial interest.

ACKNOWLEDGMENTS

This material is based upon work supported by the U.S. Army Research Laboratory and the U.S. Army Research Office under grant numbers W911NF-13-1-0424 (STIR) and W911NF-14-1-0167. We thank Dr. Brant Jones for experimental assistance and valuable scientific discussions.

REFERENCES

(1) Kelzenberg, S.; Eisenreich, N.; Eckl, W.; Weiser, V. Modelling Nitromethane Combustion. *Propellants, Explos., Pyrotech.* **1999**, *24*, 189−194.

(2) Boyer, E.; Kuo, K. K. Modeling of Nitromethane Flame Structure and Burning Behavior. *Proc. Combust. Inst.* **2007**, *31*, 2045−2053.

(3) Zhang, Y. X.; Bauer, S. H. Modeling the Decomposition of Nitromethane, Induced by Shock Heating. *J. Phys. Chem. B* **1997**, *101*, 8717−8726.

(4) Winey, J. M.; Gupta, Y. M. Shock-Induced Chemical Changes in Neat Nitromethane: Use of Time-Resolved Raman Spectroscopy. *J. Phys. Chem. B* **1997**, *101*, 10733−10743.

(5) Winey, J. M.; Gupta, Y. M. UV-Visible Absorption Spectroscopy to Examine Shock-Induced Decomposition in Neat Nitromethane. *J. Phys. Chem. A* **1997**, *101*, 9333−9340.

(6) Bouyer, V.; Darbord, I.; Herve, P.; Baudin, G.; Le Gallic, C.; Clement, F.; Chavent, G. Shock-to-Detonation Transition of Nitromethane: Time-Resolved Emission Spectroscopy Measurements. *Combust. Flame* **2006**, *144*, 139−150.

(7) Zhang, Q.; Li, W.; Lin, D. C.; He, N.; Duan, Y. Influence of Nitromethane Concentration on Ignition Energy and Explosion Parameters in Gaseous Nitromethane/Air Mixtures. *J. Hazard Mater.* **2011**, *185*, 756−762.

(8) Fried, L. E.; Manaa, M. R.; Lewis, J. P. *Adv. Ser. Phys. Chem.* **2005**, *16*, 275.

(9) Oxley, J. C. A survey of the thermal stability of energetic materials. In *Energetic Materials Part 1. Decomposition, Crystal and Molecular Properties*; Theoretical and Computational Chemistry Book Series; Elsevier: Amsterdam, 2003; Vol. *12*, p 5.

(10) Singh, R. P.; Verma, R. D.; Meshri, D. T.; Shreeve, J. M. Energetic Nitrogen-Rich Salts and Ionic Liquids. *Angew. Chem., Int. Ed.* **2006**, *45*, 3584−3601.

(11) Kozak, G. D. Factors Augmenting the Detonability of Energetic Materials. *Propellants, Explos., Pyrotech.* **2005**, *30*, 291−297.

(12) Adams, G. F.; Shaw, R. W. Chemical-Reactions in Energetic Materials. *Annu. Rev. Phys. Chem.* **1992**, *43*, 311−340.

(13) Vogelsanger, B.; Berger, B. Presented at the 36th International Annual Conference of ICT, Karlsruhe, Germany, 2005 (0/1).

(14) The NATO munitions safety information analysis centre (MSIAC).

(15) Deschambault, E.; Watt, D.; Peugeot, F.; Touze, P. Presented at the 37th International Annual Conference of ICT, Karlsruhe, Germany, 2006 (26/1).

(16) Sikder, A. K.; Sikder, N. A Review of Advanced High Performance, Insensitive and Thermally Stable Energetic Materials Emerging for Military and Space Applications. *J. Hazard Mater.* **2004**, *112*, 1−15.

(17) Badgujar, D. M.; Talawar, M. B.; Asthana, S. N.; Mahulikar, P. P. Advances in Science and Technology of Modern Energetic Materials: An Overview. *J. Hazard Mater.* **2008**, *151*, 289−305.

(18) Klerk, W. d.; Brouwer, G. R.; Keizers, H. Presented at the 37th International Annual Conference of ICT, Karlsruhe, Germany, 2006 (32/1).

(19) Bhattacharya, A.; Guo, Y. Q.; Bernstein, E. R. Nonadiabatic Reaction of Energetic Molecules. *Acc. Chem. Res.* **2010**, *43*, 1476−1485.

(20) Brill, T. B.; James, K. J. Kinetics and Mechanisms of Thermal-Decomposition of Nitroaromatic Explosives. *Chem. Rev.* **1993**, *93*, 2667−2692.

(21) Golubev, V. K. New Trends in Research of Energetic Materials. In *Proceedings of the 11th Seminar, NTREM*; University of Pardubice: Pardubice, Czech Republic, 2008; p 551.

(22) Mathieu, D. Mateo: A Software Package for the Molecular Design of Energetic Materials. *J. Hazard Mater.* **2010**, *176*, 313−322.

(23) Shterinberg, A. S.; Berlin, A. A. Presented at the 35th International Pyrotechnics Seminar, Fort Collins, Colorado, July 13-18, 2008.

(24) Beal, R. W.; Brill, T. B. Vibrational Behavior of the $-NO_2$ Group in Energetic Compounds. *Appl. Spectrosc.* **2005**, *59*, 1194−1202.

(25) Shaw, R. W.; Brill, T. B.; Thompson, D. L. *Overviews of Recent Research on Energetic Materials*; Advanced Series in Physical Chemistry; World Scientific: Singapore, 2005; Vol. *16*.

(26) Liu, K. P. Recent Advances in Crossed-Beam Studies of Bimolecular Reactions. *J. Chem. Phys.* **2006**, *125*, 132307.

(27) Lee, Y. T. In *Atomic and Molecular Beam Methods*; Oxford University Press: New York, 1987; Vol. *1*.

(28) Casavecchia, P.; Capozza, G.; Segoloni, E. *Adv. Ser. Phys. Chem.* **2004**, *14*, 329.

(29) Kaiser, R. I. Experimental Investigation on the Formation of Carbon-Bearing Molecules in the Interstellar Medium Via Neutral−Neutral Reactions. *Chem. Rev.* **2002**, *102*, 1309−1358.

DOI: 10.1021/jp5127267
J. Phys. Chem. C 2015, 119, 14653−14668

(30) Cundall, R.; Locke, A.; Street, G.; Johnson, G.; Scholes, G. *The Chemistry of Ionization and Excitation*; Taylor & Francis Ltd.: London, 1967; pp 131−140.
(31) Guo, Y. Q.; Bhattacharya, A.; Bernstein, E. R. Photodissociation Dynamics of Nitromethane at 226 and 271 nm at Both Nanosecond and Femtosecond Time Scales. *J. Phys. Chem. A* **2009**, *113*, 85−96.
(32) Sun, Y.; Shu, Y.; Xu, T.; Shui, M.; Zhao, Z.; Gu, Y.; Wang, X. Review of the Photodecomposition of Some Important Energetic Materials. *Cent. Eur. J. Energetic Mater.* **2012**, *9*, 411−423.
(33) Bass, A.; Broida, H. *Formation and Trapping of Free Radicals*. Acad Press, NY, 1960.
(34) Furman, D.; Kosloff, R.; Dubnikova, F.; Zybin, S. V.; Goddard, W. A.; Rom, N.; Hirshberg, B.; Zeiri, Y. Decomposition of Condensed Phase Energetic Materials: Interplay between Uni- and Bimolecular Mechanisms. *J. Am. Chem. Soc.* **2014**, *136*, 4192−4200.
(35) Suits, A. G. Roaming Atoms and Radicals: A New Mechanism in Molecular Dissociation. *Acc. Chem. Res.* **2008**, *41*, 873−881.
(36) Townsend, D.; Lahankar, S.; Lee, S.; Chambreau, S.; Suits, A.; Zhang, X.; Rheinecker, J.; Harding, L.; Bowman, J. The Roaming Atom: Straying from the Reaction Path in Formaldehyde Decomposition. *Science* **2004**, *306*, 1158−1161.
(37) Herath, N.; Suits, A. G. Roaming Radical Reactions. *J. Phys. Chem. Lett.* **2011**, *2*, 642−647.
(38) Bowman, J. M.; Shepler, B. C. Roaming Radicals. *Annu. Rev. Phys. Chem.* **2011**, *62*, 531−553.
(39) Nagata, T.; Suzuki, M.; Suzuki, K.; Kondow, T.; Kuchitsu, K. Λ-Doublet Populations in $CH(A_2\Delta)$ Produced in the 193 nm Multiphoton Dissociation of $(CH_3)_2CO$, $(CD_3)_2CO$, $(CH_3)_2S$ and CH_3NO_2. *Chem. Phys.* **1984**, *88*, 163−170.
(40) Napier, I. M.; Norrish, R. G. W. The Photolysis and Pyrolysis of Nitromethane and Methyl Nitrite. *Proc. R. Soc. A* **1966**, *299*, 317.
(41) Hirschlaff, E.; Norrish, R. G. W. Primary Photochemical Processes. Part IX. A Preliminary Study of the Decomposition of Nitromethane and Nitroethane. *J. Chem. Soc.* **1936**, *1580*, 1580−1585.
(42) Rockney, B. E.; Grant, E. R. Unimolecular Decomposition of Nitromethane in a Molecular Beam with Resolution of Fragment Recoil Velocities and Internal States: Dynamical Evidence for an Exit Channel Barrier. *J. Chem. Phys.* **1983**, *79*, 708.
(43) Renlund, A. M.; Trott, W. M. ArF Laser-Induced Decomposition of Simple Energetic Molecules. *Chem. Phys. Lett.* **1984**, *107*, 555−560.
(44) Mialocq, J. C.; Stephenson, J. C. Picosecond Laser-Induced Fluorescence Study of the Collisionless Photodissociation of Nitrocompounds at 266 nm. *Chem. Phys.* **1986**, *106*, 281−291.
(45) Lao, K. Q.; Jensen, E.; Kash, P. W.; Butler, L. J. Polarized Emission-Spectroscopy of Photodissociating Nitromethane at 200 and 218 nm. *J. Chem. Phys.* **1990**, *93*, 3958−3969.
(46) Moss, D. B.; Trentelman, K. A.; Houston, P. L. 193 nm Photodissociation Dynamics of Nitromethane. *J. Chem. Phys.* **1992**, *96*, 237−247.
(47) Simeonsson, J. B.; Lemire, G. W.; Sausa, R. C. Laser-Induced Photofragmentation Photoionization Spectrometry - A Method for Detecting Ambient Oxides of Nitrogen. *Anal. Chem.* **1994**, *66*, 2272−2278.
(48) Ledingham, K. W. D.; Kosmidis, C.; Georgiou, S.; Couris, S.; Singhal, R. P. A Comparison of the Femto-, Pico- and Nano-Second Multiphoton Ionization and Dissociation Processes of NO_2 at 248 and 496 nm. *Chem. Phys. Lett.* **1995**, *247*, 555−563.
(49) Greenblatt, G. D.; Zuckermann, H.; Haas, Y. OH Production in the Collision-Free UV Photolysis of Aliphatic Nitrocompounds. *Chem. Phys. Lett.* **1987**, *134*, 593−599.
(50) Wodtke, A. M.; Hintsa, E. J.; Lee, Y. T. The Observation of CH_3O in the Collision-Free Multiphoton Dissociation of CH_3NO_2. *J. Chem. Phys.* **1986**, *84*, 1044−1045.
(51) Butler, L. J.; Krajnovich, D.; Lee, Y. T.; Ondrey, G.; Bersohn, R. The Photo-Dissociation of Nitromethane at 193 nm. *J. Chem. Phys.* **1983**, *79*, 1708−1722.
(52) Wade, E. A.; Reak, K. E.; Li, S. L.; Clegg, S. M.; Zou, P.; Osborn, D. L. Time-Dependent Infrared Emission Following Photodissociation of Nitromethane and Chloropicrin. *J. Phys. Chem. A* **2006**, *110*, 4405−4412.
(53) Guo, Y. Q.; Bhattacharya, A.; Bernstein, E. R. Photodissociation Dynamics of Nitromethane at 226 and 271 nm at Both Nanosecond and Femtosecond Time Scales. *J. Phys. Chem. A* **2009**, *113*, 85−96.
(54) Hause, M. L.; Herath, N.; Zhu, R.; Lin, M.; Suits, A. G. Roaming-Mediated Isomerization in the Photodissociation of Nitrobenzene. *Nature chem* **2011**, *3*, 932−937.
(55) Goncharov, V.; Lahankar, S. A.; Farnum, J. D.; Bowman, J. M.; Suits, A. G. Roaming Dynamics in Formaldehyde-d_2 Dissociation. *J. Phys. Chem. A* **2009**, *113*, 15315−15319.
(56) Goncharov, V.; Herath, N.; Suits, A. G. Roaming Dynamics in Acetone Dissociation. *J. Phys. Chem. A* **2008**, *112*, 9423−9428.
(57) Suits, A. G.; Chambreau, S. D.; Lahankar, S. A. State-Correlated Dc Slice Imaging of Formaldehyde Photodissociation: Roaming Atoms and Multichannel Branching. *Int. Rev. Phys. Chem.* **2007**, *26*, 585−607.
(58) Fu, B.; Shepler, B. C.; Bowman, J. M. Three-State Trajectory Surface Hopping Studies of the Photodissociation Dynamics of Formaldehyde on Ab Initio Potential Energy Surfaces. *J. Am. Chem. Soc.* **2011**, *133*, 7957−7968.
(59) Zhu, R. S.; Lin, M. C. CH_3NO_2 Decomposition/Isomerization Mechanism and Product Branching Ratios: An Ab Initio Chemical Kinetic Study. *Chem. Phys. Lett.* **2009**, *478*, 11−16.
(60) Kohge, Y.; Hanada, T.; Sumida, M.; Yamasaki, K.; Kohguchi, H. Photodissociation Dynamics of Nitromethane at 213 nm Studied by Ion-Imaging. *Chem. Phys. Lett.* **2013**, *556*, 49−54.
(61) Zhu, R. S.; Raghunath, P.; Lin, M. C. Effect of Roaming Transition States Upon Product Branching in the Thermal Decomposition of Ch3no2. *J. Phys. Chem. A* **2013**, *117*, 7308−7313.
(62) Homayoon, Z.; Bowman, J. M. Quasiclassical Trajectory Study of CH_3NO_2 Decomposition via Roaming Mediated Lsomerization Using a Global Potential Energy Surface. *J. Phys. Chem. A* **2013**, *117*, 11665−11672.
(63) Dey, A.; Fernando, R.; Abeysekera, C.; Homayoon, Z.; Bowman, J. M.; Suits, A. G. Photodissociation Dynamics of Nitromethane and Methyl Nitrite by Infrared Multiphoton Dissociation Imaging with Quasiclassical Trajectory Calculations: Signatures of the Roaming Pathway. *J. Chem. Phys.* **2014**, *140*, 054305.
(64) McKee, M. L. Ab Initio Study of Rearrangements on the Nitromethane Potential Energy Surface. *J. Am. Chem. Soc.* **1986**, *108*, 5784−5792.
(65) Jacox, M. E. Photodecomposition of Nitromethane Trapped in Solid Argon. *J. Phys. Chem.* **1984**, *88*, 3373−3379.
(66) Brown, H. W.; Pimentel, G. C. *J. Chem. Phys.* **1958**, *29*, 883−888.
(67) Han, S.-p.; van Duin, A. C.; Goddard, W. A., III; Strachan, A. Thermal Decomposition of Condensed-Phase Nitromethane from Molecular Dynamics from ReaxFF Reactive Dynamics. *J. Phys. Chem. B* **2011**, *115*, 6534−6540.
(68) Guo, F.; Cheng, X.-l.; Zhang, H. Reactive Molecular Dynamics Simulation of Solid Nitromethane Impact on (010) Surfaces Induced and Nonimpact Thermal Decomposition. *J. Phys. Chem. A* **2012**, *116*, 3514−3520.
(69) Citroni, M.; Bini, R.; Pagliai, M.; Cardini, G.; Schettino, V. Nitromethane Decomposition under High Static Pressure. *J. Phys. Chem. B* **2010**, *114*, 9420−9428.
(70) Pellouchoud, L. A.; Reed, E. J. Optical Characterization of Chemistry in Shocked Nitromethane with Time-Dependent Density Functional Theory. *J. Phys. Chem. A* **2013**, *117*, 12288−12298.
(71) Reed, E. J.; Riad Manaa, M.; Fried, L. E.; Glaesemann, K. R.; Joannopoulos, J. D. A Transient Semimetallic Layer in Detonating Nitromethane. *Nat. Phys.* **2008**, *4*, 72−76.
(72) Han, S.-p.; van Duin, A. C. T.; Goddard, W. A.; Strachan, A. Thermal Decomposition of Condensed-Phase Nitromethane from Molecular Dynamics from Reaxff Reactive Dynamics. *J. Phys. Chem. B* **2011**, *115*, 6534−6540.
(73) Homayoon, Z.; Bowman, J. M.; Dey, A.; Abeysekera, C.; Fernando, R.; Suits, A. G. Experimental and Theoretical Studies of

DOI: 10.1021/jp5127267
J. Phys. Chem. C 2015, 119, 14653−14668

Roaming Dynamics in the Unimolecular Dissociation of CH_3NO_2 to CH_3O + NO. *Z. Phys. Chem.* **2013**, *227*, 1267−1280.
(74) Bowman, J. M. Roaming. *Mol. Phys.* **2014**, 1−13.
(75) Maity, S.; Kaiser, R. I.; Jones, B. M. Infrared and Reflectron Time-of-Flight Mass Spectroscopic Study on the Synthesis of Glycolaldehyde in Methanol (CH_3OH) and Methanol-Carbon Monoxide (CH_3OH−CO) Ices Exposed to Ionization Radiation. *Faraday Discuss.* **2014**, *168*, 485−516.
(76) Jones, B. M.; Kaiser, R. I. Application of Reflectron Time-of-Flight Mass Spectroscopy in the Analysis of Astrophysically Relevant Ices Exposed to Ionization Radiation: Methane (CH_4) and D4-Methane (CD_4) as a Case Study. *J. Phys. Chem. Lett.* **2013**, *4*, 1965−1971.
(77) Bennett, C. J.; Brotton, S. J.; Jones, B. M.; Misra, A. K.; Sharma, S. K.; Kaiser, R. I. High-Sensitivity Raman Spectrometer to Study Pristine and Irradiated Interstellar Ice Analogs. *Anal. Chem.* **2013**, *85*, 5659−5665.
(78) Heavens, A. S. *Optical Properties of Thin Solid Films*; Butterworthts Scientific Publications: London, 1955.
(79) Winsemius, P.; van Kampen, F. F.; Lengkeek, H. P.; van Went, C. G. Temperature Dependence of the Optical Properties of Au, Ag and Cu. *J. Phys. F: Met. Phys.* **1976**, *6*, 1583.
(80) Goodman, A. M. Optical Interference Method for the Approximate Determination of Refractive Index and Thickness of a Transparent Layer. *Appl. Opt.* **1978**, *17*, 2779−2787.
(81) Westley, M. S.; Baratta, G. A.; Baragiola, R. A. Density and Index of Refraction of Water Ice Films Vapor Deposited at Low Temperatures. *J. Chem. Phys.* **1998**, *108*, 3321−3326.
(82) Jacox, M. E., Vibrational and Electronic Energy Levels of Polyatomic Transient Molecules. In *NIST Chemistry WebBook, NIST Standard Reference Database Number 69*; Linstrom, P. J., Mallard, W. G., Eds.; National Institute of Standards and Technology: Gaithersburg, MD, 2014.
(83) Hovington, P.; Drouin, D.; Gauvin, R. Casino: A New Monte Carlo Code in C Language for Electron Beam Interaction—Part I: Description of the Program. *Scanning* **1997**, *19*, 1−14.
(84) Drouin, D.; Couture, A. R. e.; Joly, D.; Tastet, X.; Aimez, V.; Gauvin, R. Casino V2.42—A Fast and Easy-to-Use Modeling Tool for Scanning Electron Microscopy and Microanalysis Users. *SCANNING* **2007**, *29*, 92−101.
(85) Modica, P.; Palumbo, M. E. Formation of Methyl Formate after Cosmic Ion Irradiation of Icy Grain Mantles. *Astron. Astrophys.* **2010**, *519*, A22.
(86) Luna, R.; Satorre, M. Á.; Domingo, M.; Millán, C.; Santonja, C. Density and Refractive Index of Binary CH_4, N_2 and CO_2 Ice Mixtures. *Icarus* **2012**, *221*, 186−191.
(87) Hilbig, R.; Wallenstein, R. Enhanced Production of Tunable Vuv Radiation by Phase-Matched Frequency Tripling in Krypton and Xenon. *IEEE J. Quantum Electron.* **1981**, *17*, 1566−1573.
(88) Kung, A. H. Third-Harmonic Generation in a Pulsed Supersonic Jet of Xenon. *Opt. Lett.* **1983**, *8*, 24−26.
(89) Mahon, R.; McIlrath, T.; Myerscough, V.; Koopman, D. W. Third-Harmonic Generation in Argon, Krypton, and Xenon: Bandwidth Limitations in the Vicinity of Lyman-α. *IEEE J. Quantum Electron.* **1979**, *15*, 444−451.
(90) Bodenbinder, M.; Ulic, S. E.; Willner, H. A Gas-Phase and Matrix Isolation Study of the Equilibrium Ch3ono (Cis). Dblarw. Ch3ono (Trans) by Ftir Spectroscopy. *J. Phys. Chem.* **1994**, *98*, 6441−6444.
(91) Brown, H. W.; Pimentel, G. C. Photolysis of Nitromethane and of Methyl Nitrite in an Argon Matrix; Infrared Detection of Nitroxy, HNO. *J. Chem. Phys.* **1958**, *29*, 883−888.
(92) Bondybey, V.; English, J.; Mathews, C. W.; Contolini, R. Infrared Spectra and Isomerization of CHNO Species in Rare Gas Matrices. *J. Mol. Spectrosc.* **1982**, *92*, 431−442.
(93) Jacox, M. E.; Milligan, D. E. Low-Temperature Infrared Study of Intermediates in the Photolysis of HNCO and DNCO. *J. Chem. Phys.* **1964**, *40*, 2457−2460.
(94) Pettersson, M.; Khriachtchev, L.; Jolkkonen, S.; Räsänen, M. Photochemistry of HNCO in Solid Xe: Channels of UV Photolysis and Creation of H_2NCO Radicals. *J. Phys. Chem. A* **1999**, *103*, 9154−9162.
(95) Jacox, M. E. Vibrational and Electronic Energy Levels of Polyatomic Transient Molecules. Supplement A. *J. Phys. Chem. Ref. Data* **1998**, *27*, 115−393.
(96) Lowenthal, M.; Khanna, R.; Moore, M. H. Infrared Spectrum of Solid Isocyanic Acid (HNCO): Vibrational Assignments and Integrated Band Intensities. *Spectrochim. Acta, Part A* **2002**, *58*, 73−78.
(97) Bennett, C. J.; Chen, S.-H.; Sun, B.-J.; Chang, A. H. H.; Kaiser, R. I. Mechanistical Studies on the Irradiation of Methanol in Extraterrestrial Ices. *Astrophys. J.* **2007**, *660*, 1588.
(98) Maity, S.; Kaiser, R. I.; Jones, B. M. Formation of Complex Organic Molecules in Methanol and Methanol - Carbon Monoxide Ices Exposed to Ionization Radiation - A Combined FTIR and Reflectron Time-of-Flight Mass Spectrometry Study. *Phys. Chem. Chem. Phys.* **2014**, DOI: 10.1039/C4CP04149F.
(99) Jamieson, C. S.; Mebel, A. M.; Kaiser, R. I. Understand the Kinetics and Dynamics of Radiation-Induce Reaction Pathways in Carbon Monoxide Ice at 10 K. *Astrophys. J. Suppl. Ser.* **2006**, *163*, 184−206.
(100) Brunetto, R.; Caniglia, G.; Baratta, G. A.; Palumbo, M. E. Integrated Near-Infrared Band Strengths of Solid CH_4 and Its Mixtures with N_2. *Astrophys. J.* **2008**, *686*, 1480−1485.
(101) Bennett, C. J.; Jamieson, C.; Mebel, A. M.; Kaiser, R. I. Untangling the Formation of the Cyclic Carbon Trioxide Isomer in Low Temperature Carbon Dioxide Ices. *Phys. Chem. Chem. Phys.* **2004**, *6*, 735−746.
(102) Teolis, B. D.; Loeffler, M. J.; Raut, U.; Famá, M.; Baragiola, R. A. Infrared Reflectance Spectroscopy on Thin Films: Interference Effects. *Icarus* **2007**, *190*, 274−279.
(103) The integrated infrared absorptions of the methylnitrite isomer were obtained at the B3LYP/cc-pVTZ level of theory. (A.H.C. Chang, National Dong Hwa University, Taiwan).
(104) Schutte, W.; Allamandola, L.; Sandford, S. An Experimental Study of the Organic Molecules Produced in Cometary and Interstellar Ice Analogs by Thermal Formaldehyde Reactions. *Icarus* **1993**, *104*, 118−137.
(105) Gerakines, P. A.; Schutte, W. A.; Greenberg, J. M.; Van Dishoeck, E. F. The Infrared Band Strengths of H_2O, CO and CO_2 in Laboratory Simulations of Astrophysical Ice Mixtures. *Astron. Astrophys.* **1995**, *296*, 810−818.
(106) Stirling, A.; Pápai, I.; Mink, J.; Salahub, D. R. Density Functional Study of Nitrogen Oxides. *J. Chem. Phys.* **1994**, *100*, 2910−2923.
(107) Maity, S.; Kaiser, R. I.; Jones, B. M. Infrared and Reflectron Time-of-Flight Mass Spectroscopic Study on the Synthesis of Glycolaldehyde in Methanol (CH_3OH) and Methanol-Carbon Monoxide (CH_3OH-CO) Ices Exposed to Ionization Radiation. *Faraday Discuss.* **2014**, *168*, 485−516.
(108) Kaiser, R. I.; Maity, S.; Jones, B. M. Synthesis of Prebiotic Glycerol in Interstellar Ices. *Angew. Chem.* **2014**, DOI: 10.1002/anie.201408729.
(109) Afeefy, H. Y.; Liebman, J. F.; Stein, S. E. Neutral Thermochemical Data. In *NIST Chemistry Webbook, NIST Standard Reference Database*, Linstrom, P. J., Mallard, W. G., Eds.; National Institute of Standards and Technology: Gaithersburg, MD, 2010; Vol. *69*.
(110) Merkt, F.; Osterwalder, A.; Seiler, R.; Signorell, R.; Palm, H.; Schmutz, H.; Gunzinger, R. High Rydberg States of Argon: Stark Effect and Field-Ionization Properties. *J. Phys. B: At., Mol. Opt. Phys.* **1998**, *31*, 1705.
(111) Kim, Y. S.; Kaiser, R. I. On the Formation of Amines (RNH_2) and the Cyanide Anion (CN^-) in Electron-Irradiated Ammonia−Hydrocarbon Interstellar Model Ices. *Astrophys. J.* **2011**, *729*, 68−75.
(112) Kim, Y. S.; Bennett, C. J.; Li-Hsieh, C.; Brien, K. O.; Kaiser, R. I. Laboratory Studies on the Irradiation of Solid Ethane Analog Ices

DOI: 10.1021/jp5127267
J. Phys. Chem. C 2015, 119, 14653−14668

and Implications to Titan's Chemistry. *Astrophys. J.* **2010**, *711*, 744−756.
(113) Thomassy, F. A.; Lampe, F. W. A Mass Spectrometric Study of the Dimerization of Nitrosomethane. *J. Phys. Chem.* **1970**, *74*, 1188−1193.
(114) Homayoon, Z.; Bowman, J. M. Quasiclassical Trajectory Study of CH_3NO_2 Decomposition via Roaming Mediated Lsomerization Using a Global Potential Energy Surface. *J. Phys. Chem. A* **2013**, *117*, 11665−11672.
(115) Dewar, M. J. S.; Ritchie, J. P.; Alster, J. *J. Org. Chem.* **1985**, *50*, 1031.
(116) Arenas, J.; Centeno, S.; López-Tocón, I.; Peláez, D.; Soto, J. DFT and CASPT2 Study of Two Thermal Reactions of Nitromethane: C−N Bond Cleavage and Nitro-to-Nitrite Isomerization. An Example of the Inverse Symmetry Breaking Deficiency in Density Functional Calculations of an Homolytic Dissociation. *J. Mol. Struct.: THEOCHEM* **2003**, *630*, 17−23.
(117) Nguyen, M. T.; Le, H. T.; Hajgató, B.; Veszprémi, T.; Lin, M. C. Nitromethane−Methyl Nitrite Rearrangement: A Persistent Discrepancy between Theory and Experiment. *J. Phys. Chem. A* **2003**, *107*, 4286−4291.
(118) Verderame, F. D.; Lannon, J. A.; Harris, L. E.; Thomas, W. G.; Lucia, E. A. Infrared Spectra and Intermolecular Potentials of Matrix-Isolated Nitromethane and Nitromethane-d_3. *J. Chem. Phys.* **1972**, *56*, 2638−2647.
(119) Zheng, W.; Jewitt, D.; Kaiser, R. I. Electron Irradiation of Crystalline and Amorphous D_2O Ice. *Chem. Phys. Lett.* **2007**, *435*, 289−294.

DOI: 10.1021/jp5127267
J. Phys. Chem. C 2015, 119, 14653−14668